

1 **Title**

2 Dynamic dopaminergic activity controls the timing of self-timed movement

3

4 **Authors**

5 Allison E. Hamilos<sup>1†</sup>, Giulia Spedicato<sup>1†</sup>, Ye Hong<sup>1†</sup>, Fangmiao Sun<sup>2‡</sup>, Yulong Li<sup>2‡</sup> & John A.

6 Assad<sup>1,3†</sup>

7

8 **Affiliations**

9 <sup>1</sup>Department of Neurobiology, Harvard Medical School, Boston, Massachusetts, USA. <sup>2</sup>State  
10 Key Laboratory of Membrane Biology, Peking University School of Life Sciences, Beijing,  
11 China. <sup>3</sup>Istituto Italiano di Tecnologia, Genova, Italy. Correspondence should be addressed to  
12 A.E.H. ([ahamilos@mit.edu](mailto:ahamilos@mit.edu)) or J.A.A. ([jassad@hms.harvard.edu](mailto:jassad@hms.harvard.edu)).

13

14 **Current Addresses**

15 <sup>†</sup> Harvard Medical School, 220 Longwood Avenue, Warren Alpert Building Room 222, Boston,  
16 Massachusetts, 02115, USA

17 <sup>‡</sup> PKU-IDG/McGovern Institute for Brain Research, Yi He Yuan Rd#5, Beijing, 100871, P.R.  
18 China.

19

20 **Summary**

21 **Deciding when to move is a universal aspect of behavior. Pharmacological studies implicate**  
22 **the neurotransmitter dopamine as a regulator of self-timed movements, with increased**  
23 **dopamine availability generally leading to earlier movements, as if speeding an internal clock.**

24 **How dopamine affects self-timed movements is unclear; a recent study even suggested that**  
25 **increased activity in nigrostriatal dopamine neurons (DANs) is associated with *slower***  
26 **internal timing<sup>1</sup>. Here we show the dynamics of DAN activity control the timing of self-timed**  
27 **movements in mice. Animals were trained to make a self-timed lick several seconds after a**  
28 **start-timing cue. Movement times were highly variable from trial-to-trial, typical for self-**  
29 **timed actions<sup>2-6</sup>. Higher pre-trial DAN signals predicted earlier movements, consistent with**  
30 **pharmacological studies. However, surprisingly, DAN signals ramped-up over seconds**  
31 **following the start-timing cue, with the steepness of ramping predicting the trial-by-trial**  
32 **movement time. Steeply ramping signals preceded early lick-times whereas shallow ramping**  
33 **preceded later lick-times, reminiscent of a ramp-to-threshold process. Optogenetic DAN**  
34 **activation during the timed interval caused systematic early-shifting of self-timed**  
35 **movements, whereas inhibition caused systematic late-shifting. These results reveal a novel,**  
36 **causal role for dynamic DAN activity unfolding over seconds-long timescales in controlling**  
37 **the moment-by-moment decision of when to move.**

38

### 39 **Main Text**

40 Body movements can occur as short-latency reactions to external stimuli, but many movements  
41 are generated without obvious, abrupt prompting<sup>7</sup>. For example, *self-timed* movements come after  
42 a reference-timing cue, but their exact timing is highly variable from trial-to-trial relative to that  
43 cue<sup>2-6</sup>. Evidence from lesion studies and human disease implicate the nigrostriatal system in the  
44 generation of self-timed movements<sup>4,5,8,9</sup>, and pharmacological manipulations of the dopamine  
45 neurotransmitter causally influence movement timing<sup>5,8,9,10,11</sup>. For example, decreased dopamine  
46 availability/efficacy (e.g., Parkinson's disease, neuroleptic drugs) produces late-shifted self-timed

47 movements<sup>4,8</sup>, whereas high dopamine (e.g., amphetamines) produces early-shifted movements<sup>10,11</sup>,  
48 suggesting the activity of nigrostriatal dopamine neurons (DANs) may affect the speed of the  
49 internal clock.

50

51 Here, we exploited the inherent variability in the timing of self-timed movements to examine how  
52 the moment-to-moment activity of nigrostriatal DANs relates to the timing of these movements.

53 We trained head-fixed mice to make self-timed movements to receive juice rewards (Fig. 1a).

54 Animals received an audio/visual start-timing cue and then had to decide when to lick in the  
55 absence of further cues. Animals only received juice if they waited a proscribed interval following

56 the cue before making their first-lick (3.3s in most experiments). First-lick timing exhibited a broad

57 distribution spanning several seconds, as expected from previous studies<sup>3,4,5,6</sup>(Fig. 1b, Extended

58 Data Figs. 1a,b). As mice executed the task, we employed fiber photometry to record the activity

59 of genetically-defined DANs expressing the calcium-sensitive fluorophore GCaMP6f (12 mice,

60 substantia nigra pars compacta (SNc); Fig. 1c-e, Extended Data Figs. 2,3,4a). We controlled for

61 mechanical/optical artifacts by simultaneously recording fluorescence modulation of a co-

62 expressed, calcium-insensitive fluorophore, tdTomato (tdt) (Fig. 1e), as well as body movements

63 detected by neck EMG, high-speed video and a back-mounted accelerometer (Extended Data Fig.

64 5).

65

66 **DAN signals correlate with self-timing.** DAN GCaMP6f fluorescence typically exhibited brief

67 transients following cue onset and immediately before movement onset, as observed in previous

68 studies<sup>12-16</sup> (Fig. 1c). However, during the timed interval, we observed slow “ramping up” of

69 fluorescence, with a minimum after the cue-locked transient and maximum just before the lick-

70 related transient. We asked whether this ramping differed between trials in which the animal  
71 moved relatively early or late. Strikingly, when we averaged signals by movement time, we  
72 observed systematic differences in the steepness of ramping that were highly predictive of  
73 movement timing (Fig. 1d,e). Trials with early first-licks exhibited steep ramping, whereas trials  
74 with later first-licks started from lower fluorescence levels and rose more slowly toward the time  
75 of movement. The fluorescence ramps terminated at nearly the same amplitude regardless of  
76 movement time. Similar ramping dynamics and baseline differences were found in the dorsal  
77 lateral striatal “lick area<sup>17</sup>” (DLS), in both the fluorescence of GCaMP6f in DAN axon terminals  
78 (Extended Data Fig. 4b), as well as GRAB<sub>DA2m</sub> (DA<sub>2m</sub>) expressed in striatal cells (Fig. 1f, Extended  
79 Data Fig. 4c). DA<sub>2m</sub> is a new, improved extracellular dopamine indicator derived from the  
80 dopamine-2-receptor<sup>18</sup>. Thus, ramping SNc GCaMP6f dynamics are played out at the axon  
81 terminal and are reflected in striatal dopamine accumulation, suggesting that DAN ramping  
82 dynamics may causally influence movement timing via the interaction of released dopamine with  
83 downstream striatal neurons. Similar ramping dynamics were also observed in GCaMP6f-  
84 expressing DAN cell bodies in the ventral tegmental area (VTA), reminiscent of ramping dynamics  
85 observed in VTA spiking and mesolimbic dopamine release during goal-oriented navigation tasks  
86 as animals approached a rewarded target<sup>19,20</sup>(Extended Data Fig. 4d).

87  
88 In addition to ramping dynamics, slowly-modulating DAN signals were correlated with first-lick  
89 timing even before cue-onset, with higher baseline fluorescence predicting earlier first-licks (Fig.  
90 1e,f; Extended Data Figs. 4a-d, 6a-b). Because dF/F correction methods can potentially distort  
91 baseline measurements, we rigorously tested and validated three different dF/F methods, and we  
92 also repeated analyses with raw fluorescence values compared between pairs of sequential trials

93 with different movement times (Extended Data Fig. 3, Supplementary Methods A). All reported  
94 results, including the systematic baseline differences, were robust to dF/F correction. The  
95 systematic correlation of baseline signals with first-lick timing was not fully explained by prior  
96 trial outcome (reward/no reward) nor licking during the intertrial interval (ITI) (Extended Data  
97 Fig. 6c). In fact, although a reward on the prior trial tended to elevate signals during the ITI, there  
98 was an abrupt “resetting” of baseline signals during the random delay (after lamp-off but before  
99 the start-timing cue), such that baseline amplitude became abruptly and progressively better  
100 explained by the upcoming trial outcome (reward/no reward) compared to the prior trial (Extended  
101 Data Fig. 6b,c). Mice trained on a variant of the self-timing task without lamp-off/on events  
102 showed no systematic differences in their timing distributions, suggesting that although DAN  
103 resetting occurred at lamp-off, the mice still referenced their timing to the start-timing cue  
104 (Extended Data Fig. 1c).

105  
106 **Controlling for movement artifacts.** The systematic ramping dynamics and baseline differences  
107 observed with GCaMP6f and DA<sub>2m</sub> were not observed in the tdt optical control channel nor in any  
108 of the other movement-control channels (Fig. 1e; Extended Data Figs. 4e,5b), making it unlikely  
109 that these ramping dynamics could have arisen from optical artifacts. Nevertheless, because DANs  
110 show transient responses to salient cues and movements<sup>12-16</sup>, it is possible GCaMP6f and DA<sub>2m</sub>  
111 fluorescence could reflect the superposition of dopaminergic responses to multiple task events,  
112 including the cue, lick, ongoing spurious body movements, and hidden cognitive processes like  
113 timing. For example, accelerating spurious movements could, in principle, produce motor-related  
114 neural activity that “ramps up” during the timed interval, perhaps even at different rates on  
115 different trials. We thus derived a nested linear encoding model of single-trial GCaMP6f signals,

116 a data-driven, statistical approach designed to isolate and quantify the contributions of task events  
117 (timing-independent predictors) from processes predictive of movement timing (timing-dependent  
118 predictors)<sup>21,22,23</sup>(Fig. 2a,b; Extended Data Fig. 7a-d). The model robustly detected task-event  
119 GCaMP6f kernels locked to cue, lick and EMG/accelerometer events (Fig. 2c; Extended Data Fig.  
120 7e), but these timing-independent predictors alone were insufficient to capture the rich variability  
121 of GCaMP6f signals for trials with different self-timed movement times, especially the timing-  
122 dependent ramp-slope and baseline offset (68 sessions, Fig. 2c; Extended Data Fig. 7f,g). In  
123 contrast, two timing-dependent predictors robustly improved the model: 1) a baseline offset whose  
124 amplitude was linearly proportional to first-lick time; and 2) a “stretch” feature representing  
125 percentages of the interval following the cue, which predicted a ramp from cue-to-lick with slope  
126 inversely proportional to first-lick time (68 sessions, Fig. 2b,c; Extended Data Fig. 7e). Similar  
127 results were obtained for SNc DAN axon terminals in the DLS, DLS neurons expressing DA<sub>2m</sub>,  
128 and VTA DAN cell bodies (Extended Data Fig. 7h).

129  
130 In contrast to the GCaMP6f model, when the same procedure was applied to control photometry  
131 signals (tdt), the timing-independent predictors (which could potentially cause optical or  
132 mechanical artifacts—cue, first-lick, EMG/accelerometer) improved the model, but timing-  
133 dependent predictors did not improve the model (Fig. 2c; Extended Data Fig. 7f-h).

134  
135 Principle component (PC) analysis revealed ramp-like and baseline-offset-like components that  
136 explained as much as 93% of the variance in GCaMP6f signals during the timing interval (mean:  
137 66%, range: 16-93%), but similar PCs were not present in tdt signals (mean: 4%, range: 1.6-15%)  
138 (Extended Data Fig. 8a,b).

139  
140 **DAN signals predict single-trial timing.** Given that ramping and baseline-offset signals were not  
141 explained by nuisance movements or optical artifacts, we asked whether DAN GCaMP6f  
142 fluorescence could predict first-lick timing on single trials. Using a simple threshold-crossing  
143 model<sup>24</sup>, we found that the GCaMP6f signal was predictive of movement time even for low  
144 thresholds intersecting the “base” of the ramp, with the predictive value of the model progressively  
145 improving for higher thresholds ( $R^2$  low: 0.34; mid: 0.64; high: 0.94, Fig. 3a). To more thoroughly  
146 determine the independent, additional predictive power of DAN baseline and ramping signals over  
147 other task variables (e.g., movement time on previous trial; presence/absence of reward on  
148 previous trial, etc.), we derived a nested decoding model for first-lick time (Fig. 3a; Extended Data  
149 Fig. 8c). All predictors contributed to the predictive power of the model. However, even when we  
150 accounted for the contributions of prior trial history, tdt artifacts and baseline GCaMP6f signals,  
151 GCaMP6f threshold-crossing time robustly dominated the model, alone explaining 10% of the  
152 variance in first-lick time on average (range: 1-27%) (Fig. 3b-d). Alternate versions of the  
153 decoding model showed similar results (Extended Data Fig. 8c).

154  
155 **SNC DANs causally influence self-timing.** Because the DAN ramping signal robustly predicted  
156 first-lick timing and was apparently transmitted via dopamine release to downstream striatal  
157 neurons, ramping DAN activity may causally determine movement timing. If so, causally  
158 increasing the activity of DANs during timing should result in earlier self-timed movements, and  
159 vice-versa. We thus optogenetically activated or inhibited DANs (in separate experiments) on 30%  
160 of trials (Fig. 4a, Extended Data Fig. 9a,b). Activation significantly early-shifted the distribution  
161 of self-timed movements on stimulated trials compared to unstimulated trials (12 mice), whereas

162 inhibition produced significant late-shifting compared to unstimulated trials (4 mice). Stimulation  
163 of mice expressing no opsin produced no consistent effect on timing (5 mice, Figure 4b-d;  
164 Extended Data Fig. 9c-e). The direction of these effects was consistent across all animals tested in  
165 each category. Whereas bilateral stimulation of SNc DAN cell bodies caused early-shifting, the  
166 effects were generally larger and more consistent when activating SNc DAN terminals in DLS (2  
167 mice, Extended Data Fig. 9c,d). Outside the context of the timing task, DAN activation did not  
168 elicit immediate licking, nor did inhibition prevent licking, suggesting optogenetic effects on  
169 timing did not result from direct triggering or suppression of movement<sup>14</sup>, but rather were  
170 expressed through a “higher-level” cognitive process related to self-timing of the movement  
171 (Extended Data Fig. 10).

172

173 **Discussion.** Here, we found that both baseline and slowly ramping DAN signals predict the timing  
174 of self-initiated movements. Trial-by-trial differences in these signals were finely tuned to  
175 movement onset, whether these signals were recorded from SNc cell bodies, SNc terminals in the  
176 DLS, or VTA cell bodies. Moreover, slow DAN dynamics were reflected in dopamine release in  
177 DLS, demonstrating availability of this information to downstream striatal effectors positioned to  
178 influence when movement occurs. Consistent with the direction of these effects, optogenetic  
179 suppression and augmentation of DAN activity during the timing interval causally altered  
180 movement timing. Thus, DAN activity is poised to control the moment-to-moment decision of  
181 when to move.

182

183 A number of studies have reported short-latency ( $\leq \sim 500$  ms) increases in DAN activity in response  
184 to sensory cues and immediately preceding self-initiated movements<sup>12-16</sup>, similar to the sensory-

185 and motor-related transients we observed following the cue and preceding first-lick. However, the  
186 slow-timescale DAN signals we observed during self-timing were markedly different. First, the  
187 ramping signal unfolded over *seconds*, preceding the first-lick by as long as 10 s. Second,  
188 variations in baseline amplitude before the cue and the subsequent ramp-slope predicted the trial-  
189 by-trial timing of the first-lick. To effectively model DAN signals on single trials, we had to  
190 incorporate two time-dependent features: a baseline offset and a “stretch” parameter that scaled  
191 DAN signals along the time axis (Fig. 2). Moreover, these features predicted movement time  
192 independent of recent trial history (Fig. 3). Combined with the optogenetic results, these findings  
193 suggest that variations in slow DAN dynamics affect trial-by-trial movement timing.

194  
195 These slow-timescale DAN signals could be unique to the timing requirement of our task. However,  
196 when we averaged DAN signals aligned to “spontaneous” licks during the ITI, we also observed  
197 slow ramping similar to that observed during the timing interval, with signal building over seconds  
198 from the offset of the previous lick up to the time of the next lick (Extended Data Fig. 6d). Thus,  
199 slowly evolving DAN signals may be integral to self-initiated movements more generally. It is  
200 possible that slow ramping dynamics predictive of movement timing would emerge in previous  
201 datasets if DAN signals were similarly averaged according to the interval between self-initiated  
202 movement bouts.

203  
204 Previous studies have reported slow ramping signals in the mesolimbic system in certain  
205 behavioral contexts, including goal-directed navigation<sup>19</sup>; multi-step tasks culminating in  
206 reward<sup>25,26</sup>; and passive observation of dynamic visual cues indicating proximity to reward<sup>20</sup>. It has  
207 been proposed that slowly ramping mesolimbic DAN signals could encode increasing value as

208 animals approach reward<sup>25,26</sup> or alternatively could reflect moment-by-moment reward-prediction  
209 errors (RPE)<sup>20,27</sup>. The ramping signals we observed in the nigrostriatal system are consistent with  
210 either value or RPE interpretations. However, it has been unclear how the brain *employs* slowly  
211 ramping DAN signals in behavior. Our study moves beyond previous studies by finding that trial-  
212 by-trial variability in ramping dynamics explains the precise timing of a behavioral output—the  
213 self-timed lick—and that optogenetically manipulating SNc DAN activity causally alters the  
214 timing of that output. Thus, SNc ramping may not merely encode progress toward a goal, but could  
215 also play a *causal* role in the timing of movement initiation. This interpretation could be related to  
216 classic findings from Parkinson’s disease, in which loss of nigrostriatal pathway DANs results in  
217 difficulty initiating movements<sup>28,29</sup>.

218  
219 Lesion and pharmacological studies have long suggested roles for the SNc and dopamine in  
220 timing<sup>4,5</sup>. Broadly speaking, conditions that increase dopamine availability, such as amphetamine  
221 administration, affect timing as if speeding an internal “pacemaker<sup>10,11,30</sup>,” whereas conditions that  
222 decrease dopamine availability/efficacy generally have the opposite effect<sup>4,8</sup>. Our results—in both  
223 recordings and optogenetic manipulations of DANs—are consistent with this view. Moreover, the  
224 ramping signals and the anti-correlation of ramping slope with movement time bear striking  
225 resemblance to Pacemaker-Accumulator models of neural timing<sup>5,9</sup>, a longstanding conceptual  
226 framework that captures canonical features of timing behavior.

227  
228 Soares *et al.* recently reported findings complicating the standard view of dopamine in timing<sup>1</sup>. In  
229 mice performing a temporal bisection task, RPE-like transients in SNc DAN GCaMP6f signals  
230 were observed immediately after the stop-timing cue. These transients were smaller when animals

231 overestimated the timed interval, which was interpreted as evidence that *lower* DAN activity  
232 reflects a *faster* pacemaker, the *opposite* of our findings and most prior work<sup>30</sup>. This finding may  
233 be unique to the temporal bisection task, which has aspects of categorization as well as timing and  
234 thus is more complex than tasks that only rely on movement to produce timed intervals (as in our  
235 task).

236

237 However, a recently-proposed temporal difference learning framework for explaining dynamic  
238 DAN activity could provide a unified explanation for these findings<sup>20,27,30</sup>(see Supplementary  
239 Discussion for details). The model assumes that DAN activity provides a continuous readout of  
240 RPE, which under conditions of state uncertainty (as in timing) is shown to reflect the moment-to-  
241 moment derivative of the value landscape<sup>27</sup>. In this framework, variation in interval timing arises  
242 from differences in the rate of traversing the internal model of the value landscape compared to  
243 veridical time, which can be modeled as stretching/compression of the subjective value function<sup>30</sup>.  
244 Critically, the amount of compression is taken to be controlled by a pacemaker whose speed is  
245 proportional to the tonic level of dopamine from trial-to-trial<sup>30</sup>. In both the self-timed movement  
246 and bisection tasks, we observed higher *baseline* DAN signals associated with relatively fast  
247 timekeeping, consistent with relatively high tonic DAN activity reflecting fast pacemaking in both  
248 tasks. Additionally, temporally-discounted value should increase as the time of reward approaches  
249 in both tasks, and the model predicts faster pacemaking on a given trial would *compress* this  
250 function. During the self-timed movement task, compression would cause faster increases in value  
251 and thus steeper ramping of the DAN signal, as we observed. In the bisection task, compression  
252 of the value function would produce higher estimated value just before the stop-cue, and thus a  
253 smaller change in value (RPE) following the stop-cue, resulting in a blunted DAN transient. Soares

254 *et al.* indeed observed smaller stop-cue-related transients when animals overestimated the timed  
255 interval—consistent with compression of the subjective value function during fast pacemaking.

256

257 Altogether, we argue that relatively high DAN activity reflects faster pacemaking across timing  
258 tasks, with the specific timing from trial-to-trial influenced by the dynamics of DAN signaling.

259

## 260 **Main References**

261 1. Soares, S., Atallah, B. & Paton, J. Midbrain DA neurons encode perception of time. *Science*  
262 **354**, 1273–1277 (2016).

263 2. Rakitin, B. C., Penney, T. B., Gibbon, J., Hinton, S. C., & Meek, W. H. Scalar Expectancy  
264 Theory and Peak-Interval Timing in Humans. *Journal of Experimental Psychology: Animal*  
265 *Behavior Processes* **24**, 15–33 (1998).

266 3. Gallistel, C. R. & Gibbon, J. Time, Rate and Conditioning. *Psychol. Rev.* **107**, 289–344 (2000).

267 4. Merchant, H., Harrington, D. L. & Meck, W. H. Neural Basis of the Perception and Estimation  
268 of Time. *Annu. Rev. Neurosci* **36**, 313–36 (2013).

269 5. Meck, W. H. Neuroanatomical localization of an internal clock: A functional link between  
270 mesolimbic, nigrostriatal, and mesocortical dopaminergic systems. *Brain Res.* **1109**, 93–107  
271 (2006).

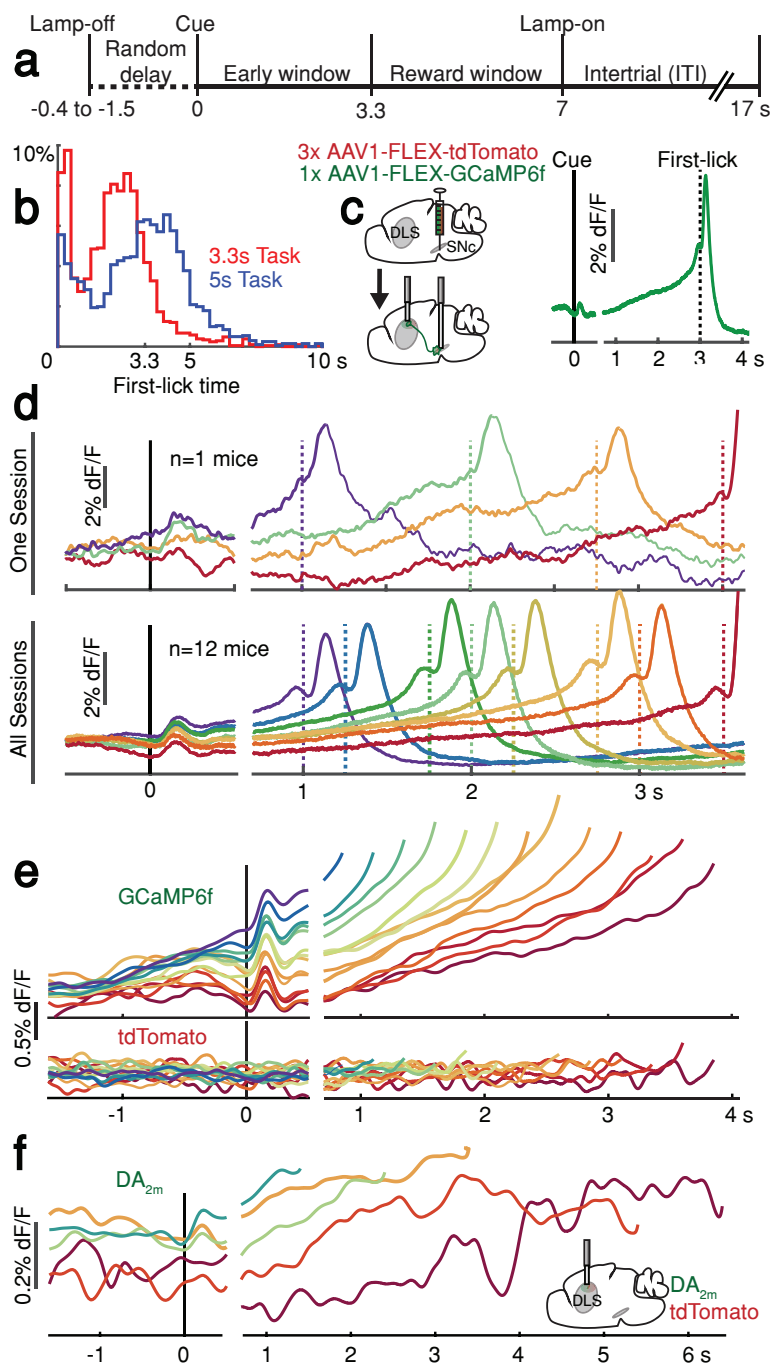
272 6. Mello, G. B. M., Soares, S. & Paton, J. J. A scalable population code for time in the striatum.  
273 *Curr. Biol.* **25**, 1113–1122 (2015).

274 7. Lee, I. H. & Assad, J. A. Putaminal Activity for Simple Reactions or Self-Timed Movements.  
275 *J. Neurophysiol.* **89**, 2528–2537 (2003).

- 276 8. Meck, W. H. Affinity for the dopamine D2 receptor predicts neuroleptic potency in decreasing  
277 the speed of an internal clock. *Pharmacol. Biochem. Behav.* **25**, 1185–1189 (1986).
- 278 9. Lustig, C. & Meck, W. H. Chronic treatment with haloperidol induces deficits in working  
279 memory and feedback effects of interval timing. *Brain Cogn.* **58**, 9–16 (2005).
- 280 10. Dews, P. B. & Morse, W. H. Some observations on an operant in human subjects and its  
281 modification by dextro amphetamine. *J. Exp. Anal. Behav.* **1**, 359–364 (1958).
- 282 11. Schuster, C. & Zimmerman, J. Timing behavior during prolonged treatment with dl-  
283 amphetamine. *J. Exp. Anal. Behav.* **4**, 327–330 (1961).
- 284 12. Schultz, W., Dayan, P. & Montague, P. R. A neural substrate of prediction and reward.  
285 *Science* **275**, 1593–1599 (1997).
- 286 13. Dodson, P. D. et al. Representation of spontaneous movement by dopaminergic neurons is  
287 cell-type selective and disrupted in parkinsonism. *Proc. Natl Acad. Sci. USA* **113**, E2180–  
288 E2188 (2016).
- 289 14. Coddington, L. T. & Dudman, J. T. The timing of action determines reward prediction  
290 signals in identified midbrain dopamine neurons. *Nat. Neurosci.* **21**, 1563–1573 (2018).
- 291 15. da Silva, J. A., Tecuapetla, F., Paixão, V. & Costa, R. M. Dopamine neuron activity before  
292 action initiation gates and invigorates future movements. *Nature* **554**, 244–248 (2018).
- 293 16. Howe, M. W. & Dombeck, D. A. Rapid signalling in distinct dopaminergic axons during  
294 locomotion and reward. *Nature* **535**, 505–510 (2016).
- 295 17. Sippy, T., Lapray, D., Crochet, S., & Petersen, C. C. H. Cell-Type-Specific Sensorimotor  
296 Processing in Striatal Projection Neurons during Goal-Directed Behavior. *Neuron* **88**, 298–  
297 305 (2015).

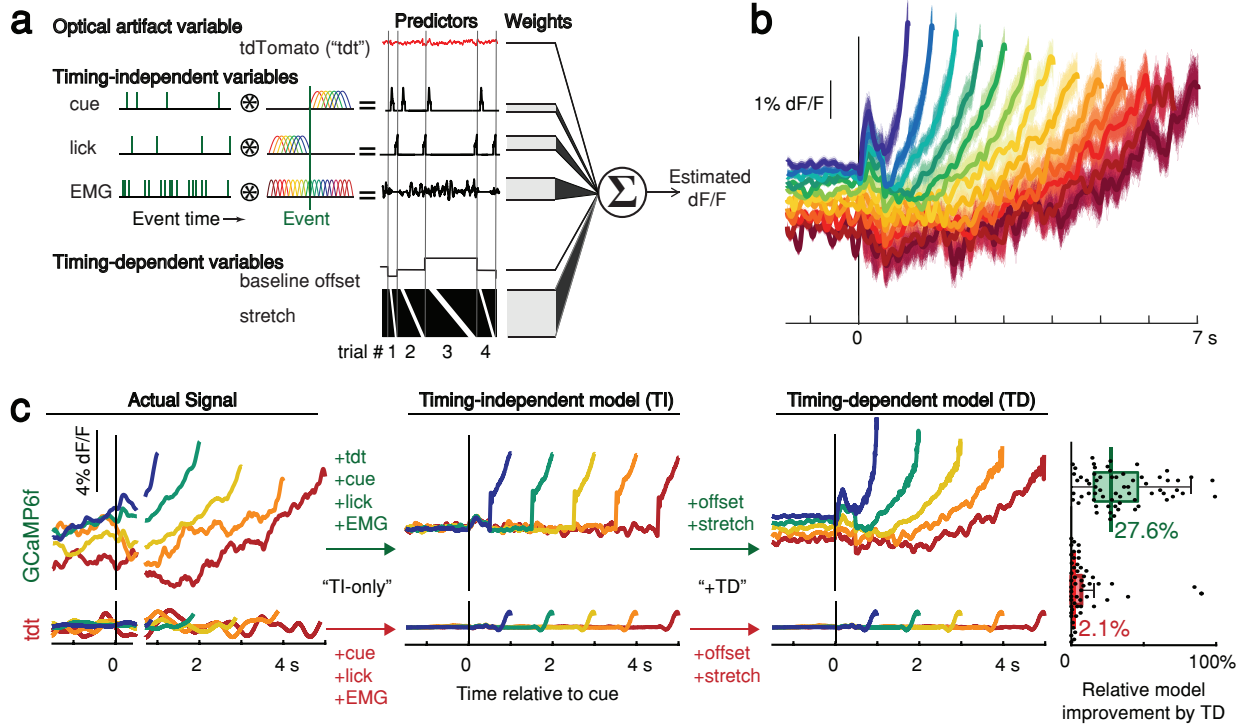
- 298 18. Sun, F. et al. New and improved GRAB fluorescent sensors for monitoring dopaminergic  
299 activity in vivo. Preprint at <https://www.biorxiv.org/content/10.1101/2020.03.28.013722v2>  
300 (2020).
- 301 19. Howe, M. W., Tierney, P. L., Sandberg, S. G., Phillips, P. E. M. & Graybiel, A. M. Prolonged  
302 dopamine signalling in striatum signals proximity and value of distant rewards. *Nature* **500**,  
303 575–579 (2013).
- 304 20. Kim, H. R. et al. A unified framework for dopamine signals across timescales. Preprint at  
305 <https://www.biorxiv.org/content/10.1101/803437v1> (2019).
- 306 21. Engelhard, B et al. Specialized coding of sensory, motor and cognitive variables in VTA  
307 dopamine neurons. *Nature* **570**, 509–513 (2019).
- 308 22. Park, I. M., Meister, M. L. R., Huk, A. C., & Pillow, J. W. Encoding and decoding in parietal  
309 cortex during sensorimotor decision-making. *Nat. Neuro.* **17**, 1395–1403 (2014).
- 310 23. Runyan, C. A., Piasini, E., Panzeri, S., & Harvey, C. D. Distinct timescales of population  
311 coding across cortex. *Nature* **548**, 92–96 (2017).
- 312 24. Maimon, G. & Assad, J. A. A cognitive signal for the proactive timing of action in macaque  
313 LIP. *Nat. Neuro.* **9**, 948–955 (2006).
- 314 25. Hamid, A. A. et al. Mesolimbic dopamine signals the value of work. *Nat. Neurosci.* **19**, 117–  
315 126 (2016).
- 316 26. Mohebi, A et al. Dissociable dopamine dynamics for learning and motivation. *Nature* **570**,  
317 65–70 (2019).
- 318 27. Mikhael, J. G., Kim, H. R., Uchida, N., & Gershman, S. J. Ramping and State Uncertainty in  
319 the Dopamine Signal. Preprint at <https://www.biorxiv.org/content/10.1101/805366v1> (2019).

- 320 28. Grillner, S. & Robertson, B. The Basal Ganglia Over 500 Million Years. *Curr. Biol.* R1088–  
321 R1100 (2016).
- 322 29. Freeze, B. S., Kravitz, A. V, Hammack, N., Berke, J. D. & Kreitzer, A. C. Control of Basal  
323 Ganglia Output by Direct and Indirect Pathway Projection Neurons. *J. Neurosci.* **33**, 18531–  
324 18539 (2013).
- 325 30. Mikhael, J. G. & Gershman, S. J. Adapting the flow of time with dopamine. *J. Neurophysiol.*,  
326 **121**, 1748–1760 (2019).
- 327
- 328
- 329
- 330
- 331
- 332
- 333
- 334
- 335
- 336
- 337
- 338
- 339
- 340
- 341
- 342
- 343



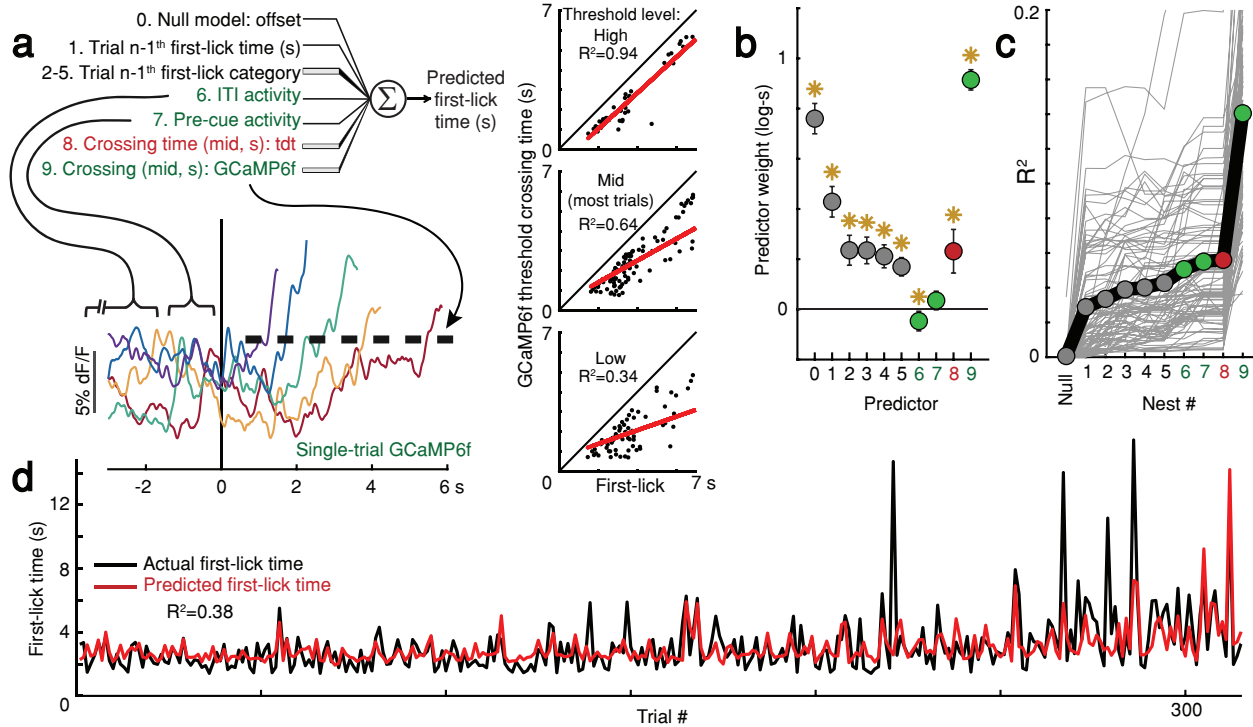
344  
345

346 **Figure 1 | Snc DAN signals preceding self-timed movement.** **a**, Self-timed movement task. **b**,  
347 First-lick distribution for two task variants performed by the same mouse. Red: 3.3 s-reward  
348 boundary (4 sessions); Blue: 5 s-reward boundary (4 sessions). For all mice, see Extended Data  
349 Fig. 1. **c**, Left: surgical strategy for GCaMP6f/tdTomato fiber photometry. Right: average Snc  
350 DAN GCaMP6f response for first-licks between 3-3.25 s (12 mice). Left of plot: cue-aligned  
351 average; right of plot: first-lick-aligned average. Vertical dashed line: first-lick time. Break in axis  
352 indicates change in plot alignment. **d**, Average Snc DAN GCaMP6f responses for different first-  
353 lick times (12 mice). **e**, Comparison of average DAN GCaMP6f and tdTomato responses (12 mice).  
354 Traces plotted up to 150 ms before first-lick. **f**, Average DLS DA<sub>2m</sub> signals (4 mice).



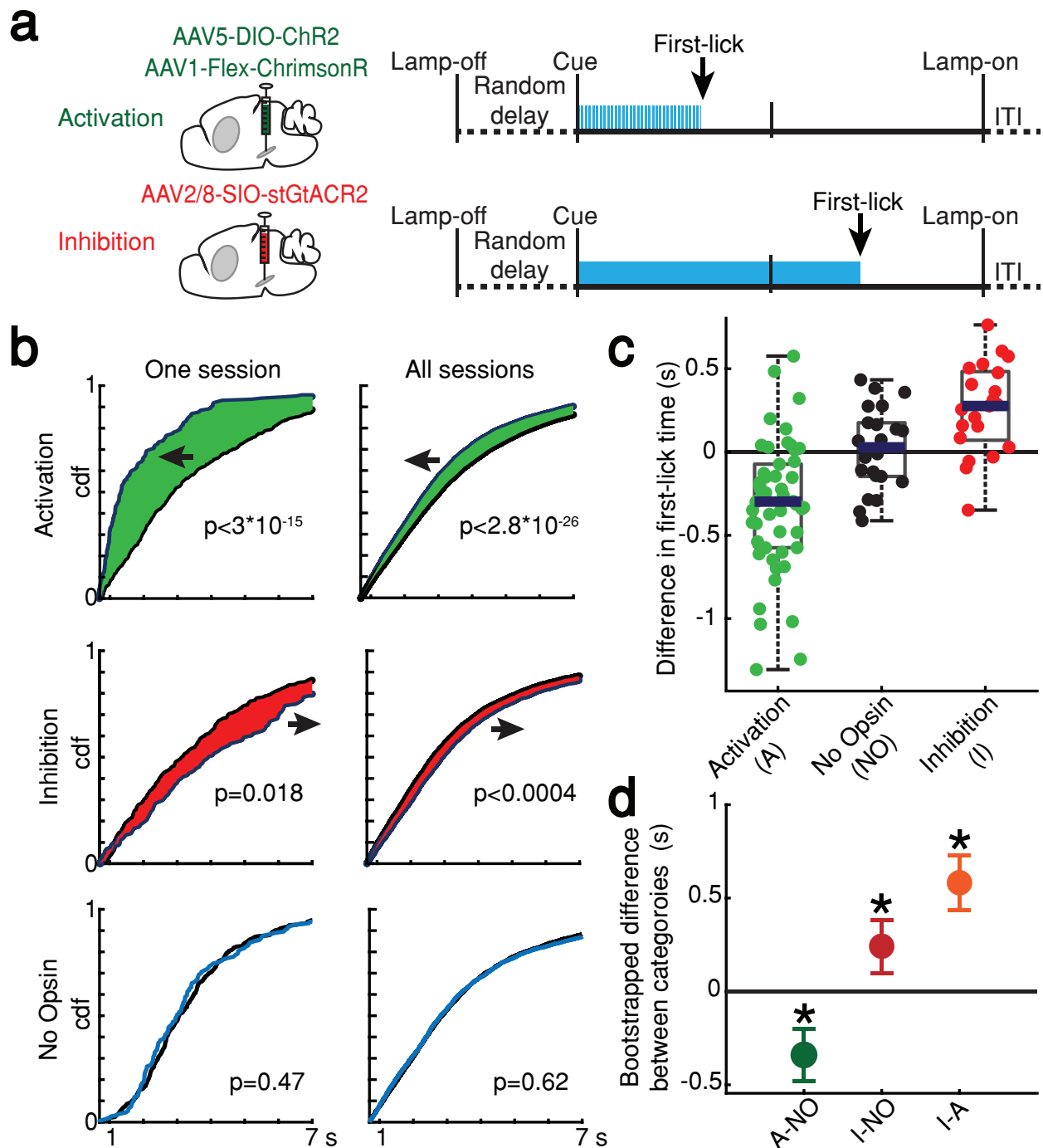
355  
 356  
 357  
 358  
 359  
 360  
 361  
 362  
 363  
 364  
 365  
 366  
 367  
 368  
 369  
 370  
 371  
 372  
 373  
 374  
 375  
 376  
 377  
 378  
 379  
 380  
 381

**Figure 2 | Contribution of optical artifacts, task variables and ongoing movements to Snc GCaMP6f signals.** **a**, Nested encoding model comparing the contribution of timing-independent predictors (TI) to the contribution of timing-dependent predictors (TD). **b**, Predicted dF/F signal for one session plotted up to time of first lick. Model error simulated 300x (shading). **c**, Nested encoding model for 1 session showing the recorded signal (left panel), the timing-independent model (middle panel), and the full, timing-dependent model with all predictors (right panel). Top: GCaMP6f; Bottom: tdTomato (tdt).



382  
383  
384  
385  
386  
387  
388  
389  
390  
391  
392  
393  
394  
395  
396  
397  
398  
399  
400  
401  
402  
403  
404  
405  
406  
407  
408

**Figure 3 | Single-trial baseline and ramping DAN signals predict first-lick timing.** **a**, Nested decoding model. Top-left: schematic. Bottom-left: single-trial cue-aligned Snc DAN GCaMP6f signals from one session (6 trials shown for clarity). Traces plotted up to first-lick. Right: threshold crossing model. Low/Mid/High: threshold amplitude. Grey dots: single trials. **b**, Model weights, 94 sessions. Error bars: 95% CI, \*:  $p < 0.05$ . Numbers indicate nesting-order. **c**, Variance explained by each model nest. Grey lines: single sessions; thick black line: average. For model selection, see **Extended Data Fig. 8c**. **d**, Predicted vs. actual first-lick time, same session as **a**.



409  
410

411 **Figure 4 | Optogenetic DAN manipulation systematically and bidirectionally shifts the timing**  
 412 **of self-timed movements.** **a**, Strategy for optogenetic DAN activation or inhibition. Mice were  
 413 stimulated from cue-onset until first-lick or 7 s. **b**, Empirical continuous probability distribution  
 414 functions (cdf) of first-lick times for stimulated (blue line) versus unstimulated (grey line) trials.  
 415 Arrow and shading show direction of effect. P-values calculated by Kolmogorov-Smirnov test (for  
 416 other metrics, see Extended Data Fig. 9b-e). **c**, Mean bootstrapped difference in first-lick time,  
 417 stimulated-minus-unstimulated trials. Dots: single sessions. **d**, Comparison of mean first-lick time  
 418 difference across all sessions. Error bars: 95% confidence interval (\*:  $p < 0.05$ ).

419 **Methods**

420 **Animals.** Adult male and female hemizygous DAT-cre mice<sup>31</sup> (B6.SJL-Slc6a3<sup>tm1.1(cre)Bkmm</sup>/J; The  
421 Jackson Laboratory) or *wt* C57/b6 mice were used in all experiments. Mice were housed on a  
422 reversed night/day cycle (12h dark/12h light) and behavioral sessions occurred during the dark  
423 cycle. All experiments and protocols were approved by the Harvard Institutional Animal Care and  
424 Use Committee and were conducted in accordance with the National Institutes of Health Guide for  
425 the Care and Use of Laboratory Animals.

426  
427 **Surgery.** Surgeries were conducted under aseptic conditions. Mice were anesthetized with  
428 isoflurane (0.5-2% at 0.8L/min). Analgesia was provided by *s.c.* 5mg/kg ketoprofen injection  
429 during surgery and once daily for 3d postoperatively. Virus was injected (50nL/min) and the pipet  
430 remained in place for 10min before removal. 200 $\mu$ m, 0.53NA blunt fiber optic cannulae (Doric)  
431 or tapered fiber optic cannulae (200 $\mu$ m, 0.60NA, 2mm tapered shank, OptogeniX) were positioned  
432 at SNc, VTA or DLS and secured to the skull with dental cement (Metabond). Neck EMG  
433 electrodes were constructed from two 32G pacemaker wires attached to a custom socket mounted  
434 in the dental cement. Sub-occipital neck muscles were exposed by blunt dissection and electrode  
435 tips embedded bilaterally.

436

437 **Stereotaxic coordinates (from bregma and brain surface).**

438 Virus:

439 SNc: 3.16mm posterior, +/- 1.4mm lateral, 4.2mm ventral

440 VTA: 3.1mm posterior, +/-0.6mm lateral, 4.2mm ventral

441 DLS: 0mm anterior, +/- 2.6mm lateral, 2.5mm ventral.

442 Fiber Optic Tips:

443 SNC/VTA: 4.0mm ventral (photometry) or 3.9mm ventral (optogenetics).

444 DLS: 2.311mm ventral (blunt fiber) or 4.0mm ventral (tapered fiber)

445

446 **Virus.**

447 Photometry:

448 tdTomato (“tdt”): AAV1-CAG-FLEX-tdT (UNC Vector Core), 100nL used alone or in

449 mixture with other fluorophores (below), working concentration  $5.3 \times 10^{12}$ gc/mL

450 gCaMP6f (at SNC or VTA): 100nL AAV1.Syn.Flex.GCaMP6f.WPRE.SV40

451 ( $2.5 \times 10^{13}$ gc/mL, Penn Vector Core). Virus was mixed in a 1:3 ratio with tdt (200nL

452 total).

453 DA<sub>2m</sub> (at DLS): 200-300nL AAV9-hSyn-DA4.4(DA2m) (working concentration: *ca.*

454  $3 \times 10^{12}$ gc/mL, Vigene) + 100nL tdt

455 Optogenetics (all bilateral at SNC):

456 ChR2: 1000nL AAV5-EF1a-DIO-hChR2(H134R)-EYFP-WPRE-pA ( $3.2 \times 10^{13}$ gc/mL,

457 UNC Vector Core)

458 ChrimsonR: 700nL AAV1-hSyn-FLEX-ChrimsonR-tdT ( $4.1 \times 10^{12}$ gc/mL, UNC Vector

459 Core)

460 stGtACR2: 300nL 1:10 AAV2/8-hSyn1-SIO-stGtACR2-FusionRed (working

461 concentration  $4.7 \times 10^{11}$ gc/mL, Addgene/Janelia Viral Core)

462

463 **Water-deprivation and acclimation.** Animals recovered 1wk postoperatively before water  
464 deprivation. Mice received daily water supplementation to maintain  $\geq 80\%$  initial body weight and  
465 fed *ad libitum*. Training commenced when mice reached the target weight ( $\sim 8$ -9d post-surgery).

466  
467 **Histology.** Mice were anesthetized with  $>400\text{mg/kg}$  pentobarbital (Somnasol) and perfused with  
468 10mL 0.9% sodium chloride followed by 50mL ice-cold 4% paraformaldehyde in 0.1M phosphate  
469 buffer. Brains were fixed in 4% paraformaldehyde at  $4^\circ\text{C}$  for  $>24\text{hr}$  before being transferred to 30%  
470 sucrose in 0.1M phosphate buffer for  $>48\text{hr}$ . Brains were sliced in  $50\mu\text{m}$  coronal sections by  
471 freezing microtome, and fluorophore expression was assessed by light microscopy. The sites of  
472 viral injections and fiber optic placement were mapped with an Allen Mouse Brain Atlas.

473  
474 **Behavioral rig, data acquisition and analysis.** A custom rig provided cues, recorded events and  
475 delivered juice rewards under the control of a Teensy 3.2 microprocessor running a custom  
476 Arduino state-system behavioral program with MATLAB serial interface. Digital and analog  
477 signals were acquired with a CED Power 1400 data acquisition system/Spike2 software  
478 (Cambridge Electronic Devices). Photometry and behavioral events were acquired at 1000Hz;  
479 movement channels were acquired at 2000Hz. Video was acquired with FlyCap2 or Spinnaker at  
480 30fps (FLIR). Data were analyzed with custom MATLAB statistics packages.

481  
482 **Self-timed movement task.** Mice were head-fixed with a juice tube positioned in front of the  
483 tongue. During periods when rewards were not available, a houselamp was illuminated. At trial  
484 start, the houselamp turned off, and a random delay ensued (0.4-1.5s) before a cue (simultaneous  
485 LED flash and 3300Hz tone, 100ms) indicated start of the timing interval. The timing interval was

486 divided into two windows, early (0-3.333s in most experiments; 0-4.95s in others) and reward  
487 (3.333-7 s; 4.95-10s), followed by the intertrial interval (ITI, 7-17 s; 10-20s). The window in which  
488 the mouse first licked determined the trial outcome (early, reward, or no-lick). An early first-lick  
489 caused an error tone (440Hz, 200ms) and houselamp illumination, and the mouse had to wait until  
490 the full timing interval had elapsed before beginning the ITI. A first-lick during the reward window  
491 caused a reward tone (5050Hz, 200ms) and juice delivery, and the houselamp remained off until  
492 the end of the trial interval. If the timing interval elapsed with no lick, a time-out error tone played  
493 (131Hz, 2s), the houselamp turned on, and ITI commenced. During the ITI and pre-cue delay,  
494 there was no penalty for licking.

495  
496 Mice learned the task in 3 stages (Extended Data Fig. 1a). On the first 1-4 days of training, mice  
497 learned a beginner-level task, which was modified in two ways: 1. To encourage participation, if  
498 mice did not lick before 5s post-cue, they received a juice reward at 5s, 2. Mice were not penalized  
499 for licking in reaction to the cue (within 500ms). When the mouse began self-triggering  $\geq 50\%$  of  
500 rewards (day 2-6 of training), the mouse advanced to the intermediate-level task, in which the  
501 training reward at 5s was omitted, and the mouse had to self-trigger all rewards. After  
502 completing  $>250$  trials/day on the intermediate task, mice advanced to the mature task (no reaction  
503 licks permitted, day 4-7 of training). All animals learned the mature task and worked for  $\sim 400$ -  
504 1500 trials/session.

505  
506 **Online movement monitoring.** Movements were recorded simultaneously during behavior with  
507 four movement-control measurements: neck EMG (band-pass filtered 50-2000Hz, 60Hz notch,  
508 amplified 100-1000x), back-mounted accelerometer (SparkFun), high-speed camera (30Hz, FLIR),

509 and tdt photometry. All control signals contained similar information, and thus only a subset of  
510 controls was used in some sessions.

511  
512 **Photometry.** Fiber optics were illuminated with 475nm blue LED light (Plexon) (SNc/VTA:  
513 50 $\mu$ W, DLS: 35 $\mu$ W) measured at patch cable tip with a light-power meter (Thor Labs). Green  
514 fluorescence was collected via a custom dichroic mirror (Doric) and detected with a Newport 1401  
515 Photodiode. Fluorescence was allowed to recover  $\geq 1$ d between recording sessions. To avoid  
516 crosstalk in animals with tdt expression, tdt was recorded at one of the 3 sites (SNc, VTA, or DLS,  
517 550 lime LED, Plexon) while GCaMP6f or DA<sub>2m</sub> was recorded simultaneously only at the other  
518 implanted sites.

519  
520 **dF/F.** Raw fluorescence for each session was pre-processed by removing rare singularities (single  
521 points  $>15$  STD from the mean) by interpolation to obtain F(t). To correct photometry signals for  
522 bleaching, dF/F was calculated as:

523

$$524 \quad \frac{dF}{F}(t) = \frac{F(t) - F_0(t)}{F_0(t)}$$

525

526 where  $F_0(t)$  is the 200 s moving average of F(t). We tested several other complementary methods  
527 for calculating dF/F and all reported results were robust to dF/F method (Supplementary Methods  
528 A). To ensure dF/F signal processing did not introduce artifactual scaling or baseline shifts, we  
529 also tested several complementary techniques to isolate undistorted F(t) signals where possible  
530 and quantified the amount of signal distortion when perfect isolation was not possible  
531 (Supplementary Methods A and Extended Data Fig. 3c.).

532

533 **Baseline DAN signal encoding models.** To determine whether baseline DAN signals were best  
534 explained by the prior trial outcome ( $n-1^{\text{th}}$ ), current trial outcome ( $n^{\text{th}}$ ), or some interaction between  
535 the two, we employed two “paired-trial” strategies, one using raw  $F(t)$  (to check for robustness to  
536  $dF/F$  scaling artifacts, Supplementary Methods A) and the other using  $dF/F$  signals. Mean baseline  
537 activity was measured in sliding windows (100ms divisions, 2s windows) from the  $n-1^{\text{th}}$  trial ITI-  
538 start to the  $n^{\text{th}}$  trial cue-onset. We abbreviate trial outcomes as E=“early” (first-lick between 0.7-  
539 3.333s, unrewarded) and R=“rewarded” (first-lick at 3.334-7s, rewarded), with the position of the  
540 letters indicating the order of consecutive trials (e.g., “ER” or “RE”).

541

542 Baseline differences between all paired, consecutive trials (EE, ER, RE, RR) were compared for  
543  $dF/F$  signals, controlling for the prior trial outcome by 4-factor ANOVA (factor 1: previous trial  
544 outcome (E or R, 1 degree of freedom (df)); factor 2: subsequent trial outcome (E or R, 1 df);  
545 factor 3: presence of licks in window (df: 1); factor 4: session ID (df: 112), comparison: baseline  
546  $dF/F$  activity within 2s sliding windows, Extended Data Fig. 6c, top). Relative influence on  
547 baseline  $dF/F$  by the  $n-1^{\text{th}}$  and  $n^{\text{th}}$  trial outcome was estimated as the relative size of the 4-way  
548 ANOVA F-statistic as a function of time (Extended Data Fig. 6c, bottom). Similar results were  
549 obtained on single sessions by 2-factor and 3-factor ANOVA. Similar results were also obtained  
550 comparing triplets of consecutive trials (EER, RRE, EEE, RRR). Both trial 2 and trial 3 in the  
551 triplet were preceded by a trial of the same outcome type, and thus we could compare baseline raw  
552  $F(t)$  signals with minimal bleaching distortion.

553

554 **DAN signal encoding model.** To test the independent contribution of each task-related input to  
555 the photometry signal and select the best model, we employed a nested fitting approach, in which  
556 each dataset was fit multiple times (in “nests”), with models becoming progressively more  
557 complex in subsequent nests. The nests fit to the GCaMP6f photometry data employed the inputs  
558  $X^{(j)}$  at each  $j^{\text{th}}$  nest:

559 Null Model:  $X^{(0)} = x_0$

560 Nest 1:  $X^{(1)} = X^{(0)} + \text{tdt}$

561 Nest 2:  $X^{(2)} = X^{(1)} + \text{cue} + \text{first-lick}$

562 Nest 3:  $X^{(3)} = X^{(2)} + \text{EMG/accelerometer}$

563 Nest 4:  $X^{(4)} = X^{(3)} + \text{time-dependent baseline offset}$

564 Nest 5:  $X^{(5)} = X^{(4)} + \text{stretch representing percentages of interval}$

565 Overfitting was penalized by ridge regression, and the optimal regularization parameter for each  
566 nest was obtained by 5-fold cross-validation to derive the final model fit for each session. Model  
567 improvement by each input was assessed by the percentage loss improvement at the nest where  
568 the input first appeared compared to the prior nest. The loss improvement of Nest 1 was compared  
569 to the Null Model (the average of the photometry timeseries). The nested model of tdt control  
570 photometry signals was the same, except Nest 1 was omitted.

571

572 The GLM for each nest takes the form:

573 
$$Y = \Theta X^{(j)}$$

574 Where  $Y$  is the  $1 \times n$  vector of the photometry signal across an entire behavioral session ( $n$  is the  
575 total number of sampled timepoints);  $X^{(j)}$  is the  $d \times n$  design matrix for nest  $j$ , where the rows

576 correspond to the  $d_j$  predictors for nest  $j$  and the columns correspond to each of the  $n$  sampled  
577 timepoints of  $Y$ ; and  $\Theta$  is the  $dxI$  vector of fit weights.

578

579  $Y$  is the concatenated photometry timeseries taken from trial start (lights off) to the time of first  
580 lick. Because of day-to-day/mouse-to-mouse variation (ascribable to many possible sources, *e.g.*,  
581 different neural subpopulations, expression levels, behavioral states, *etc.*), each session was fit  
582 separately.

583

584 The  $d_j$  design matrix predictors were each scaled (maximum amplitude 1) and grouped by input to  
585 the model. The timing-independent inputs were: 1. Null offset ( $x_0$ , 1 predictor), 2. tdt (1 predictor),  
586 3. cue (24 predictors), 4. first-lick (28 predictors), and 5. EMG/accelerometer (44 predictors). The  
587 timing-dependent inputs were: 6. timing-dependent baseline offset (1 predictor), 7. stretch (500  
588 predictors).

589

590 To reduce the number of predictors, cue, first-lick and EMG/accelerometer predictors were  
591 composed from sets of basis kernels as described previously<sup>22,23</sup>(Extended Data Fig. 7c). The cue  
592 basis kernels were spaced 0-500 ms post-cue and first-lick basis kernels were spaced -500ms-0ms  
593 relative to first-lick, the typically-observed windows of stereotypical sensory and motor-related  
594 neural responses. For nuisance movements (EMG/accelerometer), events were first discretized by  
595 thresholding (Extended Data Fig. 7b) and then convolved with basis kernels spanning -500 to 500  
596 ms around the event. This window was consistent with the mean movement-aligned optical artifact  
597 observed in the tdt channel. The timing-dependent baseline offset was encoded as a constant offset  
598 spanning from lamp-off until first-lick, with amplitude taken as linearly proportional to the timed

599 interval on the current trial. The timing-dependent stretch input was composed of 500 predictors,  
600 with each predictor containing 1's tiling 0.05% of the cue-to-lick interval, and 0's otherwise  
601 (Extended Data Fig. 7d). Importantly, the stretch was not constrained in any way to form ramps.

602  
603 Basis sets were optimized to minimize Training Loss, as calculated by mean squared error of the  
604 unregularized model:

$$605 \quad \operatorname{argmin}_{\Theta} (\text{Training Loss}(\Theta) = 1/n \sum (Y - \Theta X^{(i)})^2)$$

606  
607 Superfluous basis set elements that did not improve Training Loss compared to the Null Model  
608 were not included in the final model. Goodness of the training fit was assessed by Akaike  
609 Information Criterion (AIC), Bayesian Information Criterion (BIC),  $R^2$ , and Training Loss. The  
610 optimal, regularized model for each nest/session was selected by 5-fold cross-validation in which  
611 the regularization parameter,  $\lambda_j$ , was optimized for minimal average Test Loss:

$$612 \quad \operatorname{argmin}_{\lambda_j} (\text{Test Loss}(\Theta, \lambda_j) = 1/n \sum (Y - \Theta X^{(i)})^2 + \lambda_j |\Theta|^2)$$

613  
614 Test Loss for each optimal model was compared across nests to select the best model for each  
615 session. Models were refit with the optimal  $\lambda_j$  to obtain the final fit.

616  
617 Model error was simulated 1000 times by redrawing  $\Theta$  coefficients consistent with the data  
618 following the method described by Gelman and Hill<sup>32</sup>, and standard errors were propagated across  
619 sessions. The absolute value of each predictor was summed and divided by the total number of  
620 predictors for that input to show the contribution of the input to the model (Extended Data Fig.  
621 7g). To simulate the modeled session's photometry signal for each nest  $j$ ,  $Y_{\text{fit}}$  was calculated as

622  $\Theta X^{(i)}$  and binned by the time of first lick relative to the cue. The error in the simulation was shown  
623 by calculating  $Y_{\text{fit}_{\text{sim}}} = \Theta_{\text{sim}} X^{(i)}$  for 300 simulated sets of  $\Theta_{\text{sim}}$ .

624

### 625 **Principle component analysis (PCA)**

626 Unsmoothed ramping intervals for GCaMP6f photometry timeseries were fit with PCA and  
627 reconstructed with the first three principle components (PCs). To derive a PCA fit matrix with  
628 ramping intervals of the same number of samples, the length of each trial was scaled up by  
629 interpolation to the maximum ramping interval duration:

630  $7\text{s} - 0.7\text{s}$  cue buffer  $- 0.6\text{s}$  first-lick buffer  $= 5.7\text{s}$ : 5700 sample ramping interval

631 Following PC-fitting, datasets were down-sampled to produce a fit of the correct time duration.

632 Trials where the ramping interval was  $< 0.1\text{s}$  were excluded to exclude noise from down-sampling.

633

### 634 **First-lick time decoding model**

635 A nested, generalized linear model was derived to predict the first-lick time on each trial in a  
636 session and quantify the contribution of previous reward history and photometry signals to the  
637 prediction. The model was of the form:

$$638 \log(y) = bx$$

639 where  $b$  is a vector of fit coefficients and  $x$  is a vector of predictors. The nested model was  
640 constructed such that predictors occurring further back in time (such as reward history) and  
641 confounding variables (such as tdt photometry signals) were added first to determine the additional  
642 variance explained by predictors occurring closer to the time of first-lick, which might otherwise  
643 obscure the impact of these other variables. The predictors, in order of nesting, were:

644 Nest 0:  $b_0$  (Null model, average log-first-lick time)

645 Nest 1:  $b_1 = b_0 + \text{first-lick time on previous trial}$   
646 Nest 2-5:  $b_2 = b_1 + \text{previous trial outcome (1,0)}^*$   
647 Nest 6:  $b_3 = b_2 + \text{median photometry signal in 10s window before lamp-off}$   
648 Nest 7:  $b_4 = b_3 + \text{median photometry signal from lamp-off to cue}$   
649 Nest 9:  $b_5 = b_4 + \text{tdt threshold crossing time}^{**}$   
650 Nest 10:  $b_6 = b_5 + \text{GCaMP6f threshold crossing time}^{**}$

651

652 where all predictors were normalized to be in the interval (0,1).

653

654 \* Outcomes included (in order of nest): Reaction (first-lick before 0.5s), Early (0.5-3.333s),  
655 Reward (3.333-7s), ITI (7s-17s). No-lick was implied by all four outcomes encoded as zeros.

656 \*\* Details on threshold-crossing time and alternative models included in Supplementary Methods

657 B.

658

659 To exclude the sensory- and motor-related transients locked to the cue and the first-lick events in  
660 the threshold-crossing nests, the ramping interval was conservatively defined as 0.7s post-cue up  
661 until 0.6s before first-lick, and the minimum ramping interval for fitting was 0.1s. Thus, for a trial  
662 to be included in the model, the first lick occurred between 1.4s to 17s (end of trial).

663

664 Initial model goodness of fit was assessed by  $R^2$ , mean-squared loss and BIC. Models were 5-fold  
665 cross-validated with ridge regression at each nest to derive the final models, as described above.  
666 95% confidence intervals on model coefficients were calculated by 2-sided t-test with standard  
667 errors propagated across sessions.

668

669 **Optogenetics—naïve/expert control sessions.** To determine whether optogenetic stimulation  
670 directly elicited or prevented licking, licking behavior was first tested outside the context of the  
671 self-timed movement task on separate sessions in the same head-fixed arena but with no cues or  
672 behavioral task. Opsin-expressing mice were tested before any exposure to the self-timed  
673 movement task (“Naïve”) as well as after the last day of behavioral recording (“Expert”). In Chr2  
674 control sessions, stimulation (5mW 425nm light, 3s duration, 10Hz, 20% duty cycle) was applied  
675 randomly at the same pace as in the self-timed movement task. stGtACR2 control sessions were  
676 conducted similarly (12mW 425mW light, 3s duration, constant illumination); but to examine if  
677 inhibition could block ongoing licking, we increased the baseline lick-rate by delivering juice  
678 rewards randomly (5% probability checked once every 5s).

679

680 **Optogenetics—self-timed movement task.** SNc DANs were optogenetically manipulated in the  
681 context of the 3.3s self-timed movement task. To avoid over-stimulation, light levels were adjusted  
682 to be subthreshold for eliciting overt movements<sup>14</sup>, and mice were not stimulated on consecutive  
683 days.

684

685 Activation: SNc cell bodies were illuminated bilaterally (Chr2: 0.5-5mW 425nm blue LED light;  
686 ChrimsonR 550nm lime or 660nm crimson) on 30% of trials (10Hz, 20ms up-time starting at  
687 cue onset and terminating at first-lick). DAN terminals in DLS were stimulated bilaterally via  
688 tapered fiber optics on separate sessions.

689 Inactivation: SNc cell bodies were illuminated bilaterally (stGtACR2: 12 mW 425 nm blue light)  
690 on 30% of trials (constant illumination starting at cue onset and terminating at first lick).

691

692 **Quantification of optogenetic effects.** The difference in the distribution of trial outcomes between  
693 stimulated and unstimulated trials on *each session* was quantified in four ways.

694 1. 2-Sample Unsigned Kolmogorov-Smirnov Test.

695 2. Difference in empirical continuous probability distribution function (cdf). The difference  
696 in the integral of the stimulated and unstimulated cdf (dAUC) was calculated for each  
697 session from 0.7-7s. Effect size was quantified by permutation test, wherein the identity of  
698 each trial (stimulated or unstimulated) was shuffled, and the distribution of dAUCs for the  
699 permuted cdfs was calculated 10,000x. Results were reported for all sessions.

700 3. Difference in mean movement time. Movement times on stimulated and unstimulated trials  
701 were pooled and the distribution of movement time differences was determined by non-  
702 parametric bootstrap, in which a random stimulated and unstimulated trial were drawn from  
703 their respective pools 1,000,000x and the difference taken. The mean of each session's  
704 bootstrapped distribution was compared across sessions by the 1,000,000x bootstrapped  
705 difference of the mean between sessions of different categories.

706 4. Difference in median movement time. Same as above but with median.

707

#### 708 **Code availability**

709 All custom behavioral software and analysis tools are available  
710 at <https://github.com/harvardschoolofmouse>.

711

#### 712 **Data availability**

713 The data that support the findings of this study are available from the corresponding author upon  
714 reasonable request.

715

## 716 **Methods references**

717 31. Backman, C. M *et al.* Characterization of a Mouse Strain Expressing Cre Recombinase From  
718 the 3' Untranslated Region of the Dopamine Transporter Locus. *Genesis* **44**, 383–390 (2006).

719 32. Gelman, A., & Hill, J. *Data Analysis Using Regression and Multilevel/Hierarchical Models*.  
720 Cambridge University Press, Cambridge, 43-45 (2006).

721

## 722 **Acknowledgements**

723 We thank D. Chicharro, J.G. Mikhael, S.J. Gershman, S. Panzeri and E.N. Brown for discussions  
724 on analytical methods; V. Berezovskii, J. LeBlanc, T. LaFratta, O. Mazor, P. Gorelik, J. Markowitz,  
725 A. Lutas, K.W. Huang, and N.E. Ochandarena for technical assistance; and B. Sabatini, C. Harvey,  
726 S.R. Datta, M. Andermann and W. Regehr for reagents. The work was supported by NIH grants  
727 UF-NS109177 and U19-NS113201, and NIH core grant EY-12196. A.E.H. was supported by a  
728 Harvard Lefler Predoctoral Fellowship and a Harvard Quan Predoctoral Fellowship.

729

## 730 **Author Contributions**

731 A.E.H. and J.A.A conceived the project. A.E.H. performed all experiments. G.S. assisted with  
732 experiments using tapered fiber optics; Y.H. assisted with optogenetics control experiments. F.S.

733 and Y.L. developed the dopamine sensor, DA<sub>2m</sub>. A.E.H. and J.A.A. analysed the data and wrote  
734 the paper.

735

736 **Competing Interests**

737 J.A.A. is a co-founder of OptogeniX, which produces the tapered optical fibers used in some  
738 experiments.

739

740 **Extended Data** is available for this paper.

741

742 **Supplementary Information** including Supplementary Methods and Discussion are available  
743 for this paper.

744

745 **Correspondence and requests for materials** should be addressed to A.E.H. or J.A.A.

746

747

748

749

750

751

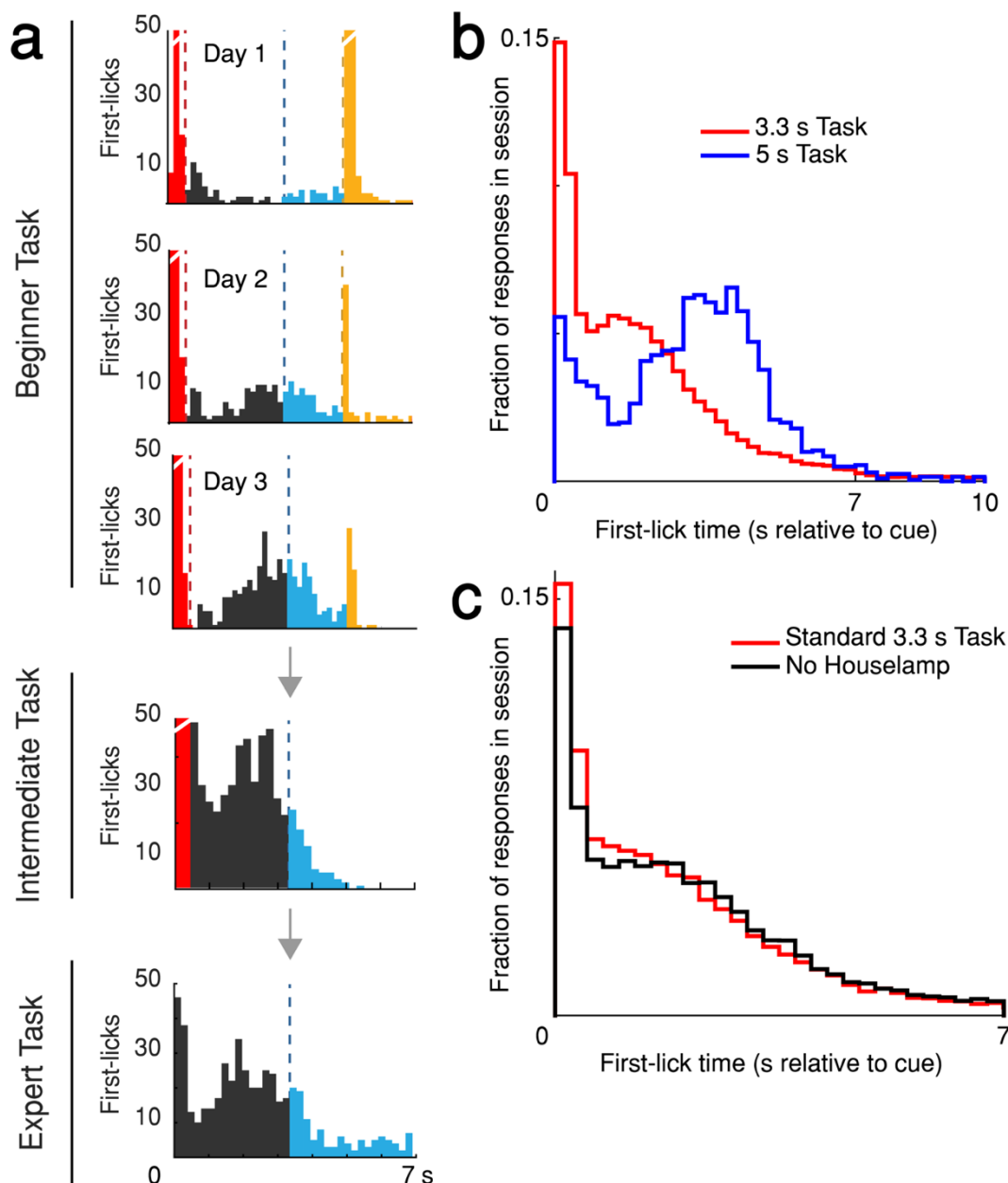
752

753

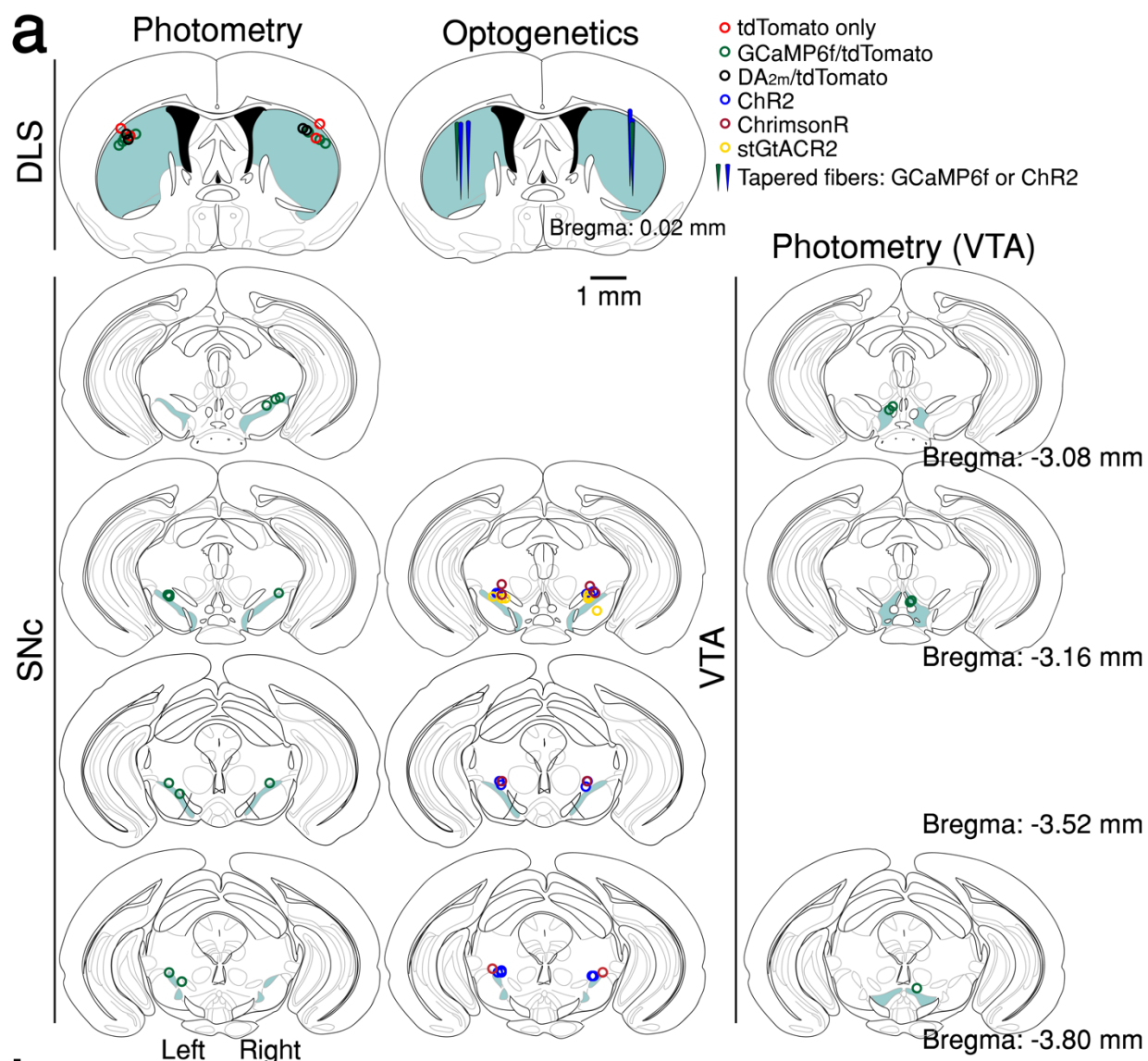
754

755

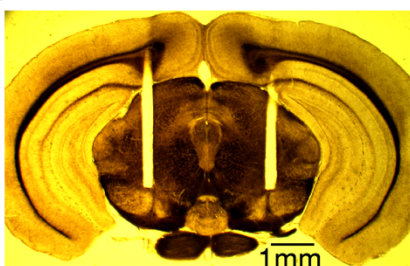
756 **Extended Data**



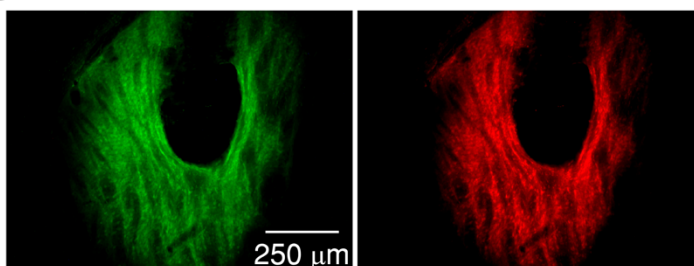
757 **Extended Data Figure 1 | Self-timed movement task learning and variations.** **a**, Task learning.  
758 Histogram of first-licks from single sessions at different stages of training. Bar color indicates first  
759 lick category (red: reaction, grey: early, blue: operant-rewarded, gold: Pavlovian-rewarded).  
760 Diagonal slash across bar top indicates bar height truncated for clarity. **b**, First-lick distributions  
761 from tasks with different target timing intervals (16 mice, 152 sessions). Red: 3.3 s reward-  
762 boundary. Blue: 5 s reward-boundary. Mice adjust behavior to the timing-contingencies of the  
763 task. **c**, First-lick distributions during behavior with and without houselamp cues. Red: standard  
764 3.3 s task; Black: 3.3 s task omitting houselamp cues (4 mice, 4-5 sessions/mouse on each version  
765 of the task). Mice time their first-licks relative to the start cue, not the houselamp.  
766



**b**

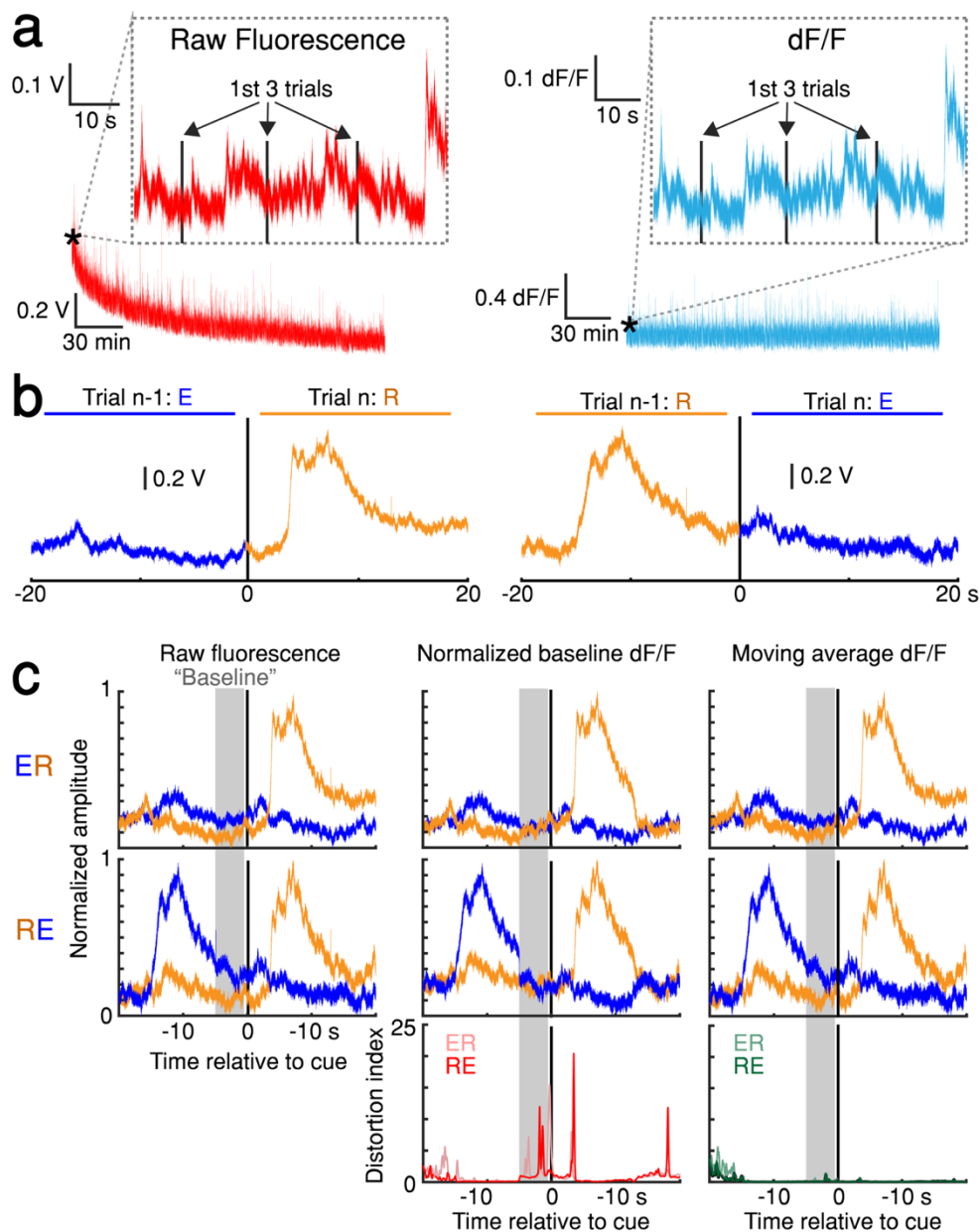


**c**

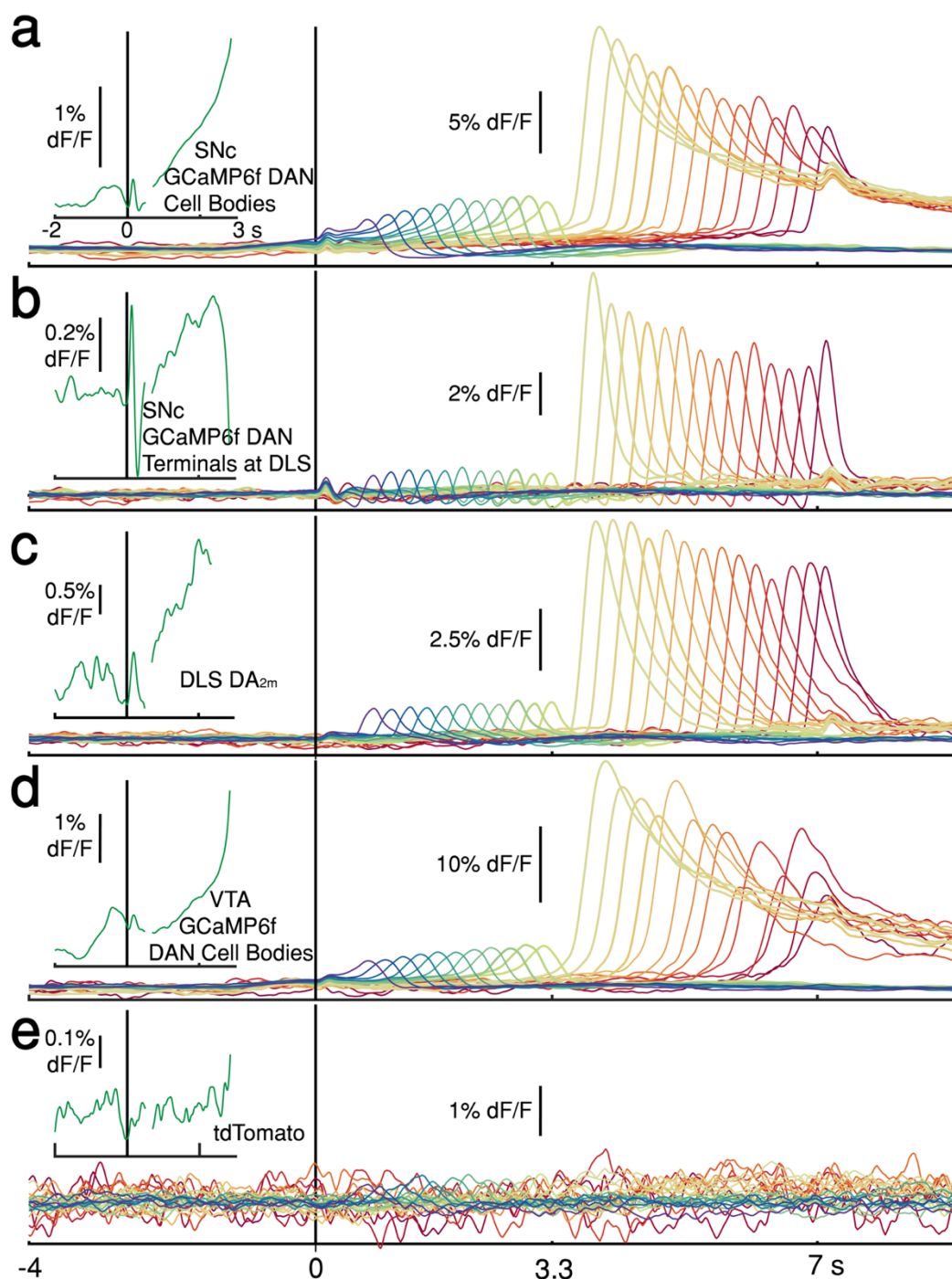


767  
768

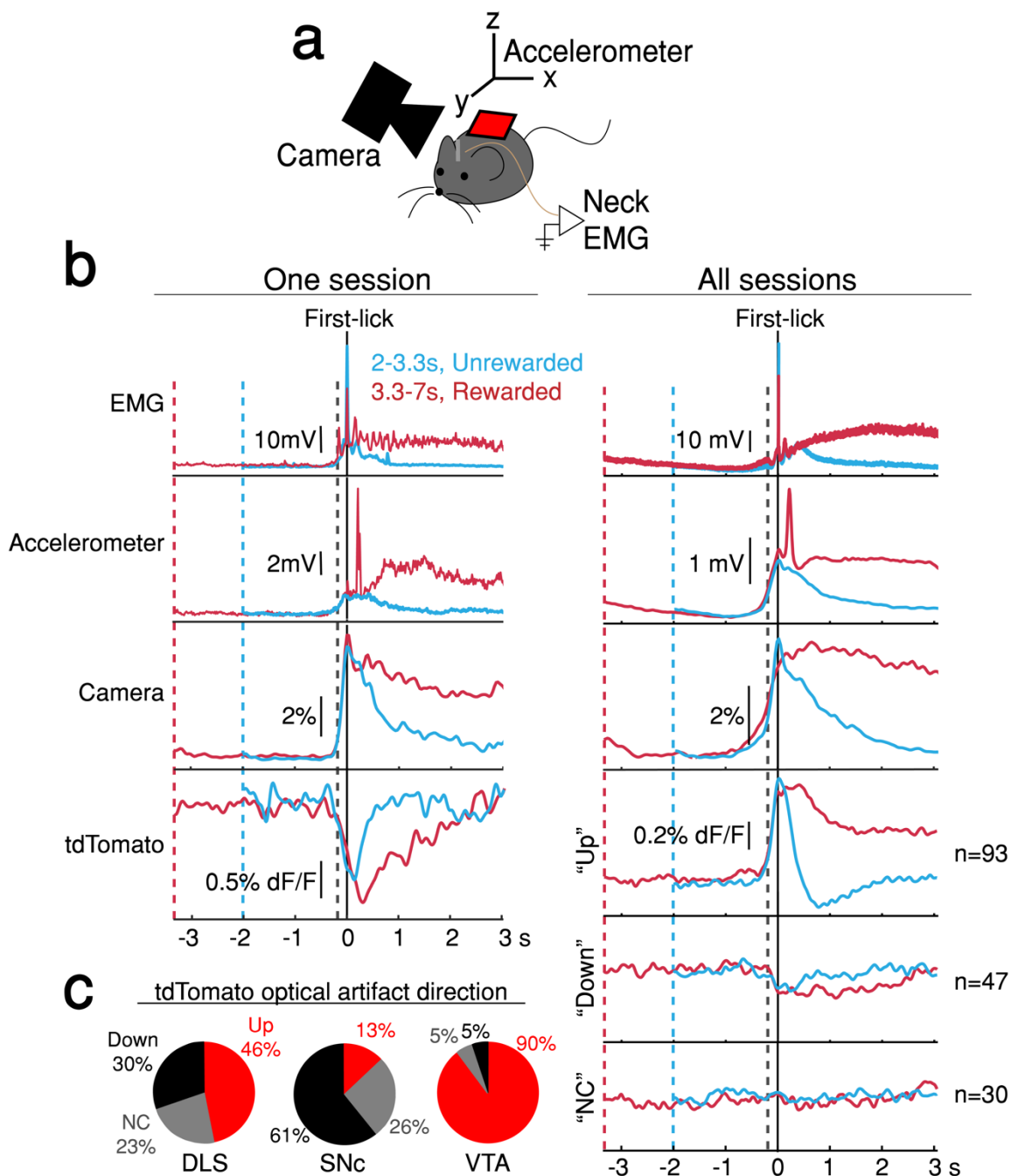
769 **Extended Data Figure 2 | Fiber optic placement and histology.** **a**, Approximate fiber positions,  
770 all mice. **b**, Brightfield microscopy with polarized filter on a freshly-cut brain slice showing  
771 bilateral fiber placement at SNC (stGtACR2). **c**, Example of co-expression of green and red  
772 fluorophores relative to fiber optic tip (Left: DA<sub>2m</sub>, Right: tdTomato).



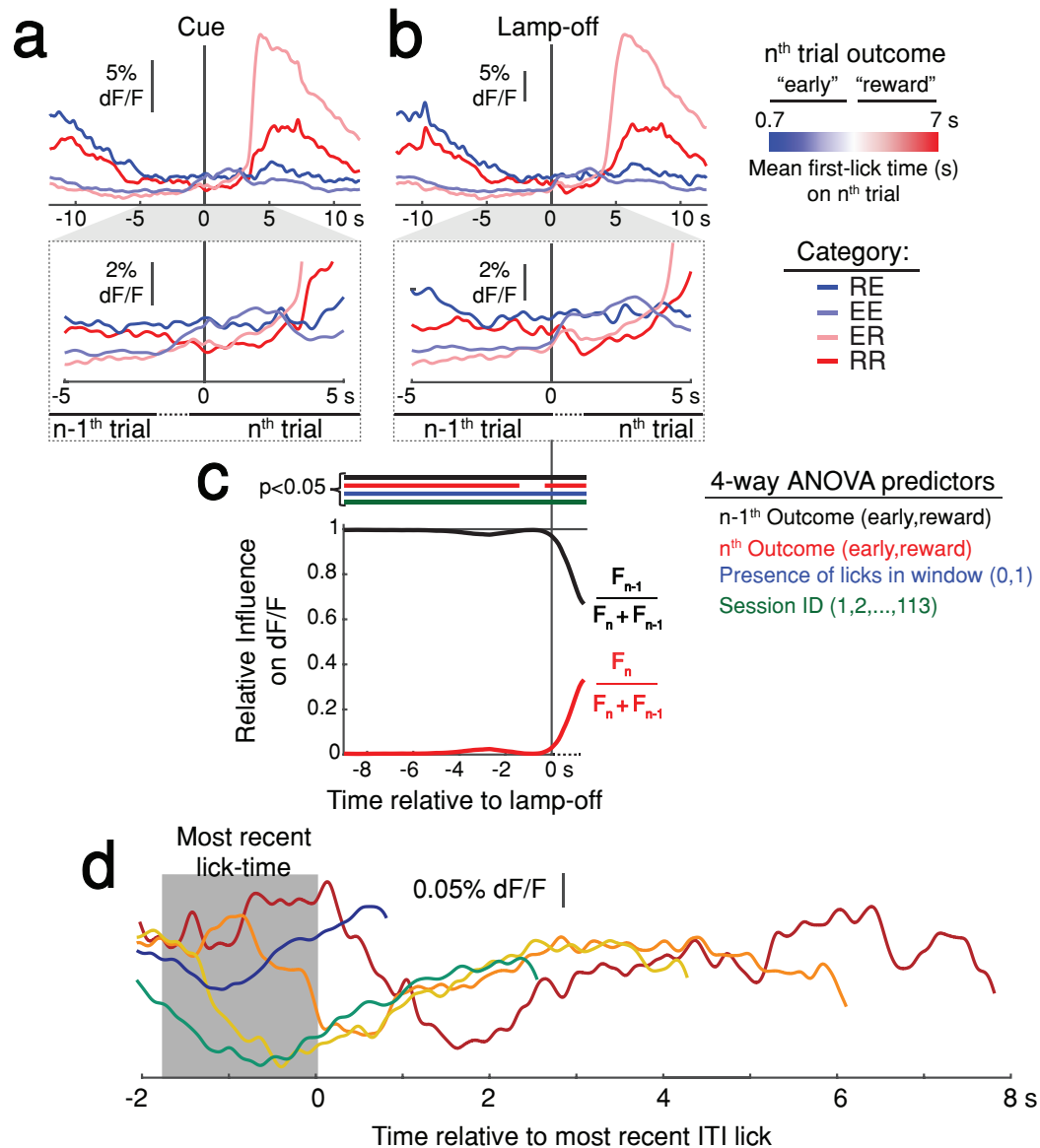
773  
 774 **Extended Data Figure 3 | dF/F method validation.** **a**, Minimal bleaching occurs over a 3-trial  
 775 window. Left: slow, raw fluorescence bleaching across one session. Left inset: Comparison to  
 776 bleaching across the first 3 trials (~1 min). Right: dF/F removes bleaching dynamics. Right inset:  
 777 the same 3-trial window shown for dF/F-treated signal. **b**, Average raw fluorescence on paired,  
 778 consecutive trials from one session aligned to cue on the  $n^{\text{th}}$  trial. Left:  $n-1^{\text{th}}$  trial was early,  $n^{\text{th}}$  trial  
 779 was rewarded ("ER" condition). Right: "RE" condition (See Supplementary Methods A). **c**.  
 780 Comparison of baseline GCaMP6f signals on paired, consecutive trials aligned to cue. Columns:  
 781 three different versions of the signal (Raw fluorescence, Normalized baseline dF/F method,  
 782 Moving average dF/F method). Top row: ER condition; middle row: RE condition; bottom row:  
 783 distortion index. Red distortion index plot shows only Normalized baseline method. Green  
 784 distortion index plot shows overlay of Moving Average, Low-Pass Filter, and Multiple Baseline  
 785 dF/F Methods because the difference in signal distortion between these methods was  
 786 indistinguishable (See Supplementary Methods A).



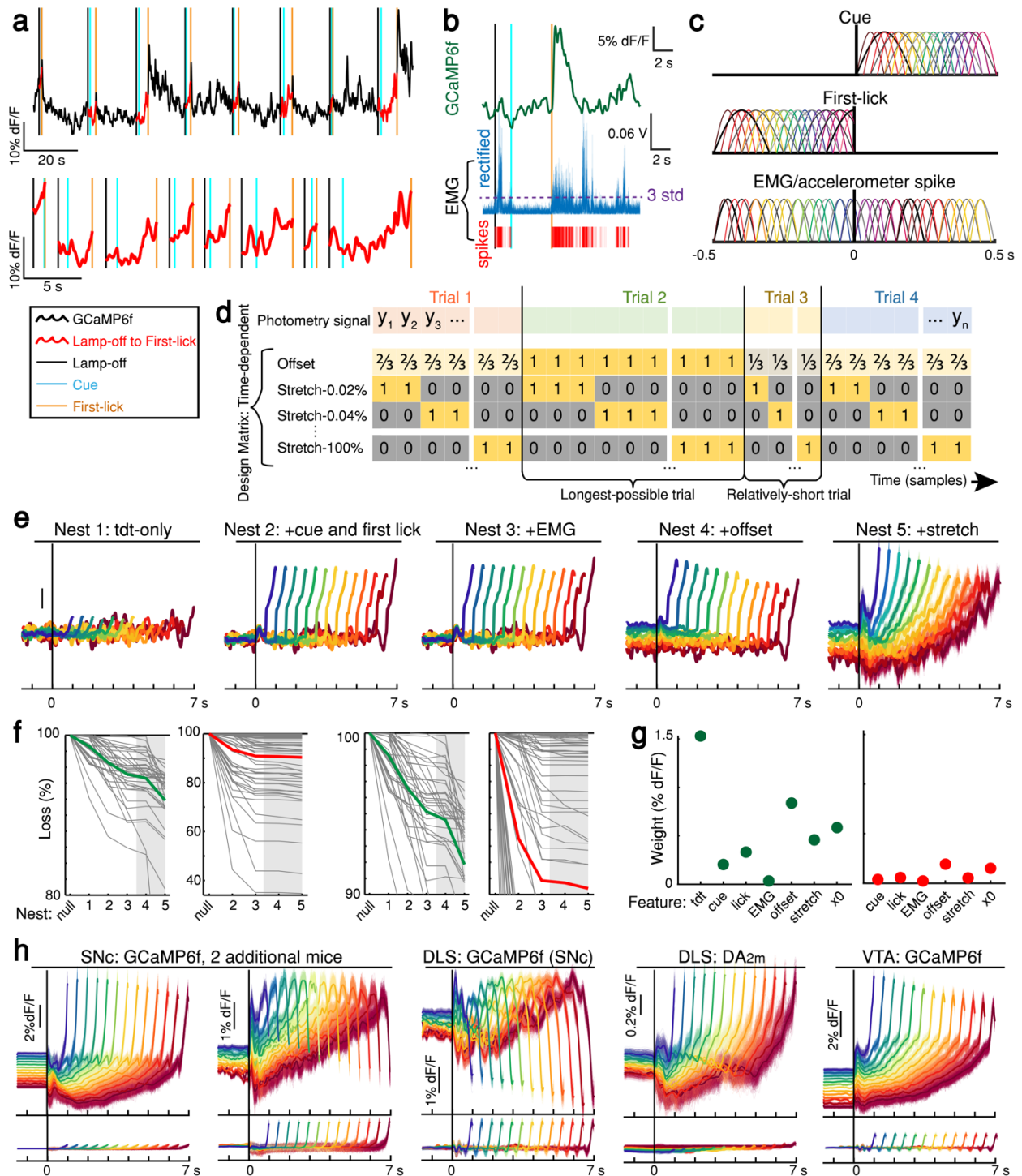
787  
 788 **Extended Data Figure 4 | Cue-aligned average photometry signals showing reward-related**  
 789 **responses: all mice, all fluorophores. a,** DAN GCaMP6f signals at SNc cell bodies (12 mice). **b,**  
 790 DAN GCaMP6f signals at axon terminals in DLS. The sharp, downward deflection immediately  
 791 prior to movement onset was observed in every mouse (12/12) on every session and was not  
 792 explained by movement artifacts. There appears to be a rapid “off” response. **c,** Striatal DA<sub>2m</sub>  
 793 signals at DLS (4 mice). **d,** DAN GCaMP6f signals at VTA cell bodies (4 mice). **e,** tdTomato  
 794 signals (all sites, all sessions). **Insets:** Average signals for first-licks occurring between 3-3.25,  
 795 aligned to cue (left of axis break) and aligned to first-lick (right of axis break). Traces plotted up  
 796 till approximate movement onset (150 ms before first-lick).



797  
798 **Extended Data Figure 5 | Movement controls reliably detect movements, but there is no**  
799 **systematic difference in movement before first-lick during the timing interval. a**, Schematic  
800 of movement controls. **b**, First-lick-aligned average movement signals on rewarded (red) and  
801 unrewarded (blue) trials. Pre-lick traces are truncated at the nearest cue-time for the averaged  
802 traces (dashed red, dashed blue). Left: one session; Right: all sessions. Dashed grey line: time of  
803 earliest-detected movement on most sessions (150 ms before first-lick). Average first-lick-locked  
804 tdt optical artifacts showed inconsistent directions even within the same session. Averages for all  
805 three types of artifact (consistently up, “Up”; consistently down, “Down”; and not consistent “NC”)  
806 shown for all sessions. **c**, Breakdown of average tdt artifact direction by session at each recording  
807 site.

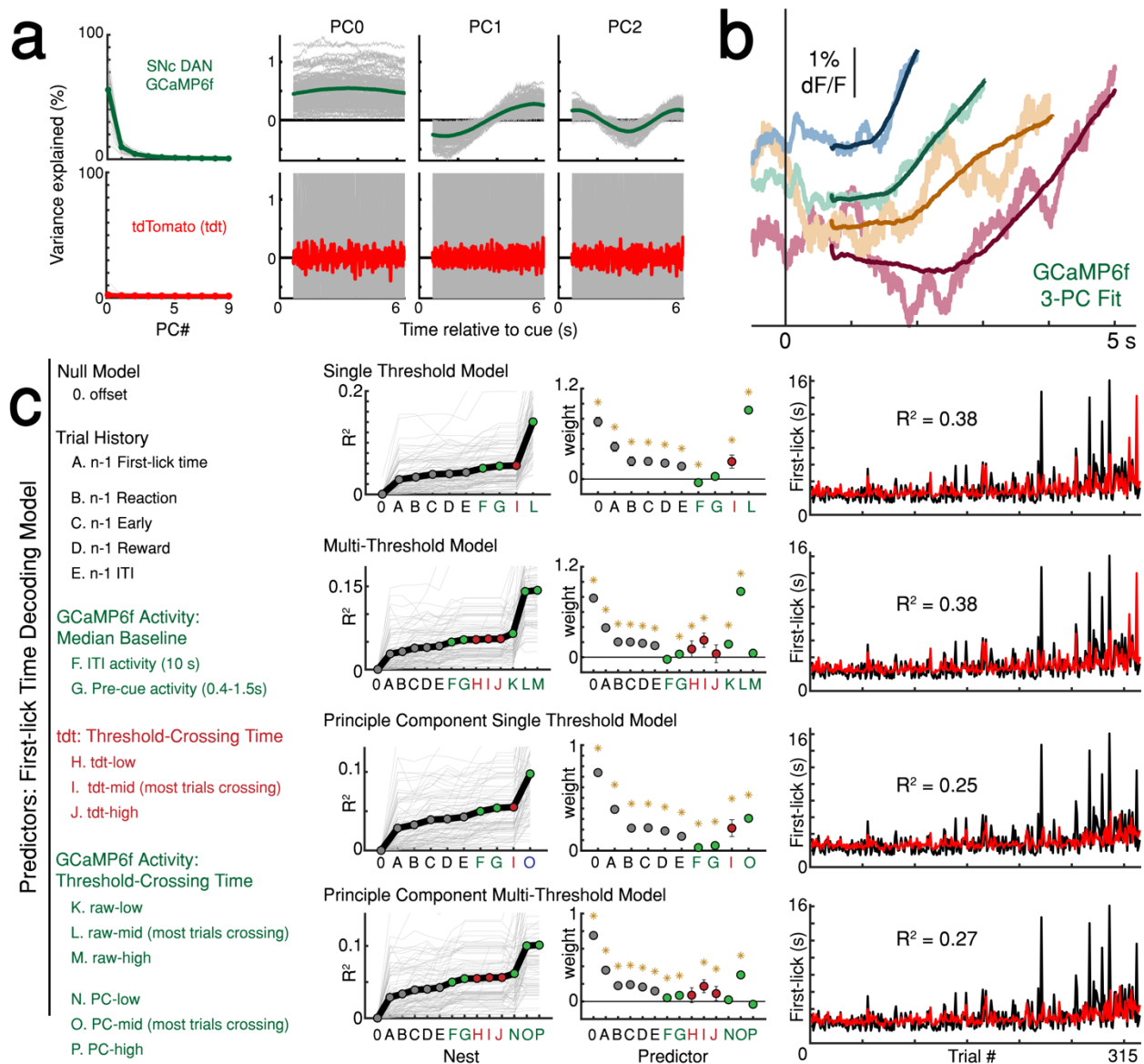


808  
 809 **Extended Data Figure 6 | Baseline SNc DAN signals predict trial outcome, even when**  
 810 **controlling for prior trial outcome and ongoing movement.** Paired, consecutive trials were  
 811 pooled into 4 categories based on the  $n-1^{\text{th}}$  and  $n^{\text{th}}$  trial outcomes (4 mice, the 17 sessions with  
 812 highest signal to noise and number of trials). Categories: Early-Early (EE, where  $n-1^{\text{th}}$  outcome is  
 813 early,  $n^{\text{th}}$  outcome is early: 2254 trials), Early-Reward (ER: 730 trials), Reward-Early (RE: 190  
 814 trials) and Reward-Reward (RR: 174 trials). To control for the contribution of movement to  
 815 baseline signals, plots are shown only for trials with no licking during the last 5 seconds of the ITI  
 816 before Lamp-off. **a**, Cue-aligned average DAN signals become more predictive of  $n^{\text{th}}$  trial outcome  
 817 as the cue time approaches. **b**, Lamp-off-aligned average DAN signals show “resetting” effect  
 818 after the houselamp turns off. Before lamp-off, average DAN signals reflect the  $n-1^{\text{th}}$  trial outcome;  
 819 subsequently they reflect the  $n^{\text{th}}$  trial outcome. **c**, Selectivity index taken on single trials quantifies  
 820 the relative contribution of  $n-1^{\text{th}}$  and  $n^{\text{th}}$  trial outcomes to the prediction of the baseline signal.  
 821 (Index calculated to exclude timepoints after the  $n^{\text{th}}$  trial first-lick). **d**, Average ITI GCaMP6f  
 822 signals aligned to most recent previous lick-time plotted up to onset of next spontaneous self-  
 823 initiated lick during the ITI. (1 mouse, 5 sessions, truncated 150 ms before lick detection).



824  
 825 **Extended Data Figure 7 | DAN GCaMP6f signal encoding model parameterization and**  
 826 **model selection.** **a**, Schematic of photometry timeseries fit by encoding model. The lamp-off to  
 827 first-lick interval was isolated from each trial in a session (top) and concatenated to produce the  
 828 timeseries fit by the model (bottom). **b**, Derivation of EMG spikes from raw signals. Thresholding  
 829 of rectified EMG at 3 standard deviations (std) during an example trial. **c**, Optimized basis kernels  
 830 for cue, first-lick, and EMG/accelerometer spikes to produce timing-independent features. **d**,  
 831 Schematic of  $d \times n$  Design Matrix for timing-dependent features. Note: timing-independent

832 features not shown for clarity in schematic. **e**, GCaMP6f model fits by nest for example session.  
833 Model error simulated 300x (shading). **f**, Model loss by nest. Green: mean loss for SNc GCaMP6f;  
834 red: mean loss for tdTomato (tdt); grey lines: individual sessions; grey shading: timing-dependent  
835 nests. Left: full-scale view of all datasets. Right: mean GCaMP6f and tdt loss compared on same  
836 scale. **g**, Summary of feature weights across SNc GCaMP6f (left) and tdt (right) models (68  
837 sessions each). Coefficient weights were rectified, summed, and divided by the number of  
838 predictors per feature. Error bars: 2\*standard error (too small to see). All features were significant  
839 in both GCaMP6f and tdt models. **h**, Top: examples of the full timing-dependent model (nest 5)  
840 from additional mice for all recording conditions. Bottom: tdt control channel fit. Model errors  
841 simulated 300x. Some mice show downward-going movement-related spikes at SNc cell bodies  
842 (second panel). All mice showed downward-going movement-related spikes from SNc terminals  
843 in DLS (middle panel).  
844  
845  
846  
847



848

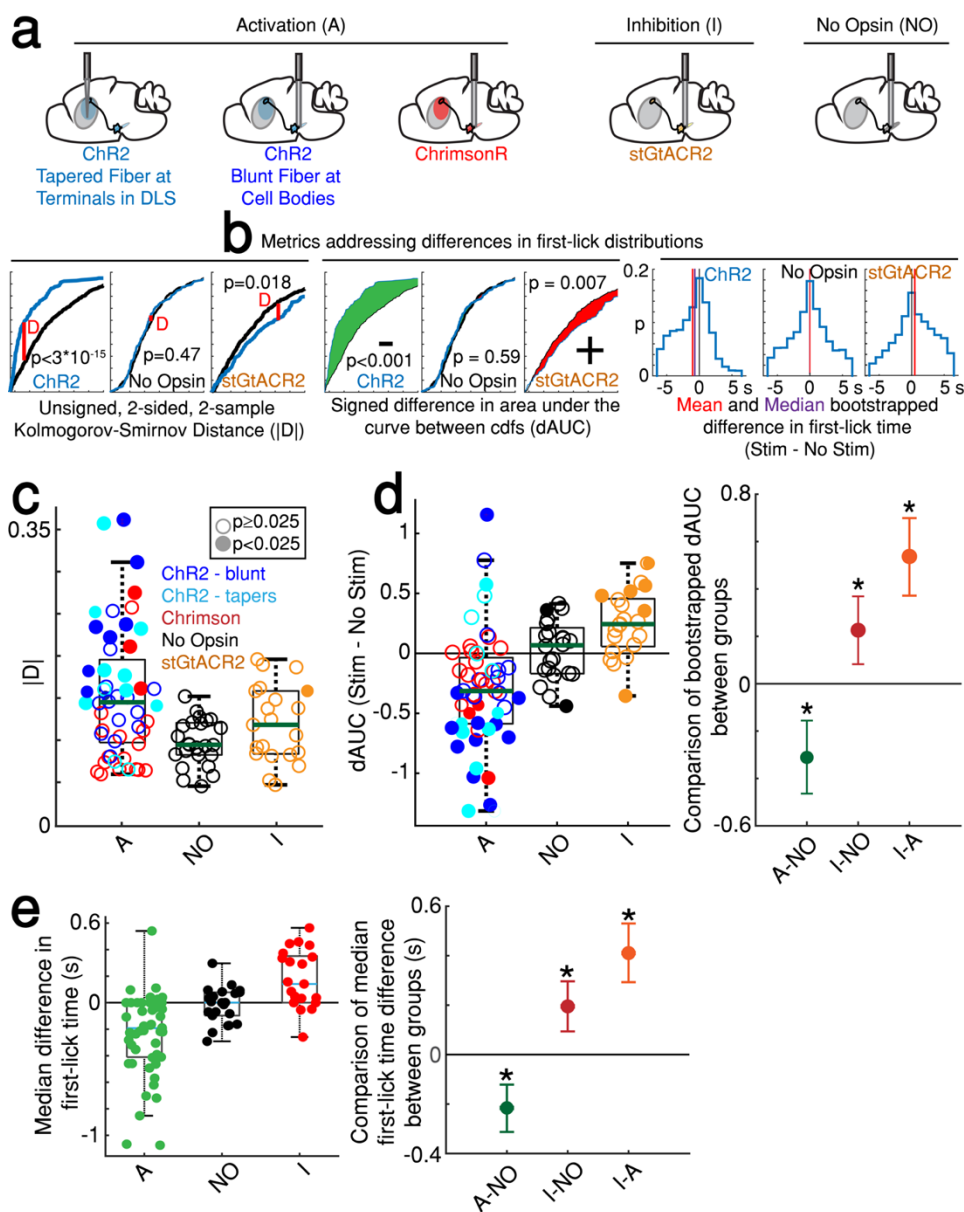
849

850 **Extended Data Figure 8 | Variations of the first-lick time decoding model.** **a**, Principle  
 851 component analysis (PCA) of the ramping interval (0.7 s up to first-lick relative to cue). Green:  
 852 mean GCaMP6f recorded at SNc; Red: mean tdTomato (tdt) recorded at SNc and VTA; Grey lines:  
 853 single-session data. Left: Variance explained by first 10 principle components (PC). Right: Scores  
 854 of first three principle components. X-axis shown for longest-possible interpolated trial duration;  
 855 trials of shorter duration were interpolated to have the same number of samples for PCA. **b**,  
 856 Example session data simulated with first 3 PCs. Light traces: actual averaged GCaMP6f activity  
 857 truncated at first-lick onset; Dark traces: PC fits of the same trials. **c**, Decoding model variations.  
 858 \*:  $p < 0.05$ , error bars: 95% confidence intervals. GCaMP6f threshold crossing time dominated  
 859 every version of the model; n-1<sup>th</sup> trial first-lick time was consistently the second-best predictor.

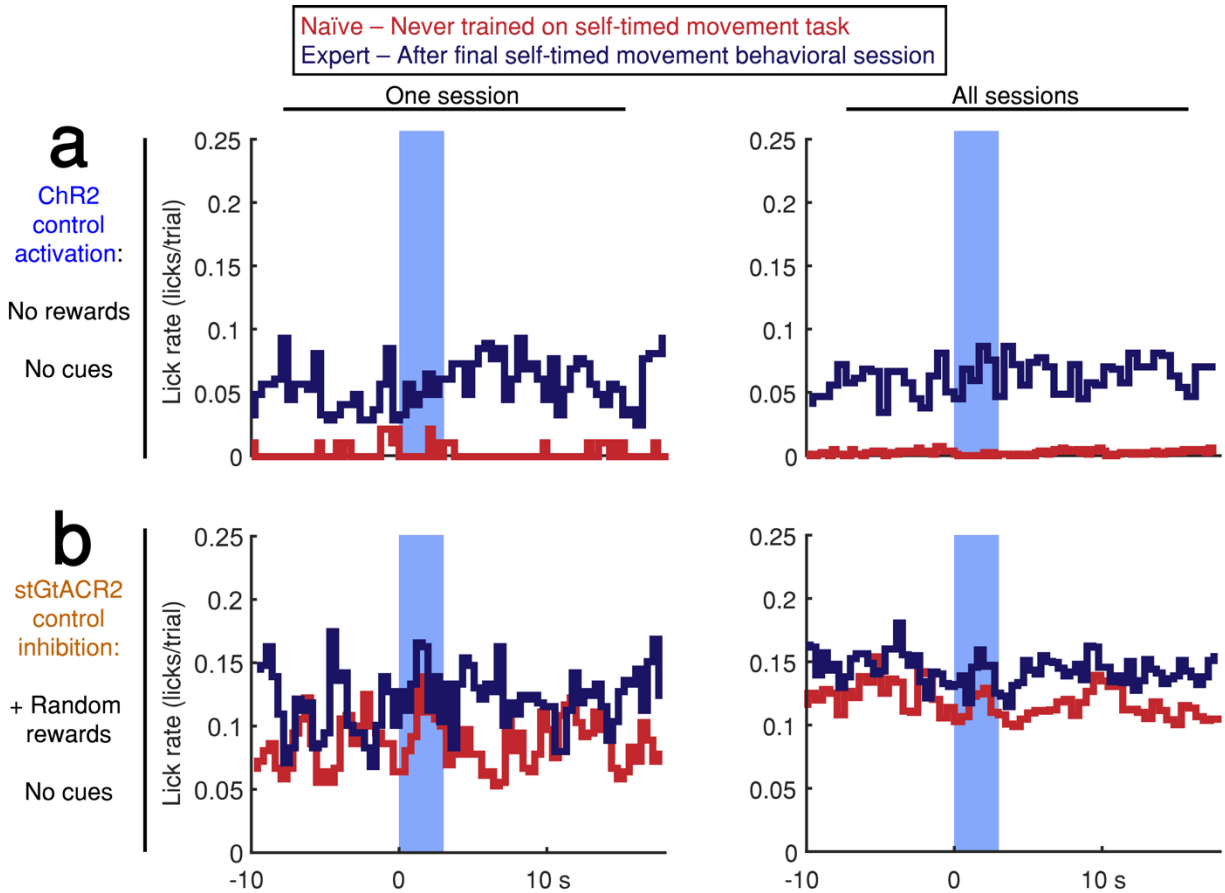
860

861

862



863  
864 **Extended Data Fig. 9 | Variations on measurements of optogenetic effects.** **a**, Strategy for  
865 optogenetic targeting of DANs. **b**, Comparison of four complementary metrics for addressing  
866 optogenetic effects. Left: unsigned Kolmogorov-Smirnov Distance (KS-D) assay of differences in  
867 first-lick time distribution. Center: signed, bootstrapped comparison of difference in area under  
868 the cdf curves (dAUC). Right: mean and median bootstrapped difference in first-lick time. **c**, KS-  
869 D Assay: all sessions. A: activation sessions; NO: no opsin sessions; I: inhibition sessions. Filled  
870 circles indicate significant difference between stimulated/unstimulated trials on single session  
871 ( $p < 0.025$ , 2-sided, 2-sample KS test). **d**, Left: bootstrapped dAUC Assay: all sessions. Filled  
872 circles: significant difference on single session ( $p < 0.025$ , 2-sided bootstrapped dAUC test, see  
873 Methods). Right: comparison of dAUC in first-lick distributions across all sessions between groups.  
874 Error bars denote bootstrapped 95% confidence interval (\*:  $p < 0.05$ ). **e**, Left: median bootstrapped  
875 difference in first-lick time, stimulated-minus-unstimulated trials. Dots indicate single sessions.  
876 Comparison of median difference in first-lick time across all sessions. Error bars denote  
877 bootstrapped 95% confidence interval (\*:  $p < 0.05$ ).



878

879 **Extended Data Figure 10 | Optogenetic DAN stimulation does not cause or prevent licking.**

880 **a,b** Stimulation-aligned lick-rate during stimulation-control sessions. Animals expressing ChR2

881 or stGtACR2 were tested in 1-3 control sessions both before exposure to the self-timed movement

882 task (red) and in 1-2 control sessions after the end of behavioral training (red). Blue bar indicates

883 stimulation period (3 s starting at time 0 s). Left: one control session, Right: all sessions. **a,**

884 Activation control sessions (no cues or rewards). Animals were head-fixed on the behavioral

885 platform in the absence of any cues or rewards and were stimulated randomly at the same pace as

886 the standard 3.3 s self-timed movement task. Activation did not elicit immediate licking in any

887 single session. **b,** Inhibition-control sessions (no cues, + random rewards). Animals were head-

888 fixed on the behavioral platform in the absence of cues while receiving juice rewards at random

889 times. Inhibition did not prevent licking in any single session.

890

891

892

893

894

895

896 **Supplementary Information**

897 **1. Supplementary Methods.....p46-51**

898 A. dF/F method characterization and validation.....p46-49

899 B. Derivation of threshold and alternative decoding models.....p49-51

900 **2. Supplementary Discussion.....p52-72**

901 **3. Supplementary References.....p72-73**

902

903 **1. Supplementary Methods**

904

905 **A. dF/F method characterization and validation**

906 dF/F calculations are intended to reduce the contribution of slow fluorescence bleaching to fiber

907 photometry signals, and many such methods have been described<sup>1,20,26</sup>. However, dF/F methods

908 have the potential to introduce artifactual distortion when the wrong method is applied in the wrong

909 setting. Thus, to derive an appropriate dF/F method for use in the context of the self-timed

910 movement task, we characterized and quantified artifacts produced by 4 candidate dF/F techniques.

911

912 ***Detailed description of complementary dF/F methods.***

- 913 1. Normalized baseline: a commonly used dF/F technique in which each trial's
- 914 fluorescence is normalized to the mean fluorescence during the 5 s preceding the trial.
- 915 2. Low-pass digital filter:  $F_0$  is the low-pass, digital infinite impulse response (IIR)-
- 916 filtered raw fluorescence for the whole session (implemented in MATLAB with the
- 917 built-in function *lowpass* with  $f_c=5 \cdot 10^{-5}$  Hz, steepness=0.95).

- 918 3. Multiple baseline: a variation of Method 1, in which each trial's fluorescence is  
919 normalized by the mean fluorescence during the 5 s preceding the current trial, as well  
920 as 5 trials before the current trial and 5 trials after the current trial.
- 921 4. Moving average:  $F_0$  is the 200 s moving average of the raw fluorescence at each point  
922 (100 s on either side of the measured timepoint).

923

924 Although *normalized baseline* (Method 1) is commonly used to correct raw fluorescence signals  
925 (F) for bleaching, this technique assumes that baseline activity has no bearing on the type of trial;  
926 however, because the mouse decides when to move in the self-timed movement task, it is possible  
927 that baseline activity may differ systematically with the mouse's choice on a given trial. Thus,  
928 normalizing F to the baseline period would obscure potentially physiologically-relevant signals.  
929 More insidiously, if baseline activity *does* vary systematically with the mouse's timing,  
930 normalization can also introduce substantial amplitude scaling and y-axis shifting artifacts when  
931 correcting F with this method (Extended Data Fig. 3c, middle panel). Thus, Methods 2-4 were  
932 designed and optimized to isolate photometry signals minimally distorted by bleaching signals and  
933 systematic baseline differences during the self-timed movement task. Methods 2-4 produced the  
934 same results in all statistical analyses, and the moving average method is shown in all figures.

935

936 ***Isolating minimally-distorted photometry signals with paired trial analyses of raw fluorescence.***

937 Although slow bleaching prevents comparison of raw photometry signals (F) at one time in a  
938 behavioral session with those at another time, the time-course of appreciable bleaching was slow  
939 enough in the reported behavioral sessions that minimal bleaching occurred over the course of 3  
940 trials (~1 min, Extended Data Fig. 3a). Thus, F was comparable on sets of *paired* trials. To observe

941 the most minimally-distorted photometry signals possible, average F on paired trials was compared  
942 (Extended Data Fig. 3b,c). Because dF/F baseline DAN signals were systematically related to lick  
943 timing, we compared F baseline signals between all paired trials in which an Early (first-lick  
944 between 0.7-2.9s, unrewarded) trial was followed by a Late (first-lick between 3.4-7s, rewarded)  
945 trial (“ER” comparison). To ensure systematic differences did not result from subtle bleaching in  
946 the paired-trial interval, we reversed the ordering contingency and also compared all Late trials  
947 preceding Early trials (“RE comparison”). The same systematic relationship between baseline  
948 signals and first-lick time was found for paired trials analyzed by raw F (Extended Data Fig. 3c,  
949 left panel).

950

951 ***Quantification of artifactual amplitude scaling/baseline shifts introduced by dF/F processing.***

952 Each Candidate dF/F Method was applied to the same Paired Trial datasets described above. The  
953 resulting paired-fluorescence datasets were normalized after processing (minimum dF/F=0,  
954 maximum=1). The amount of distortion introduced by dF/F was quantified with a Distortion Index  
955 (DI), which was calculated as:

956 
$$\text{Distortion Index, DI}(t) = \text{abs}(F(t) - dF/F(t))$$

957 where F(t) and dF/F(t) are the normalized, paired-trial raw fluorescence signal or dF/F signal at  
958 time t, respectively. t spanned from the beginning of the n-1<sup>th</sup> trial (-20 s) to the end of the n<sup>th</sup> trial  
959 (20s), aligned to the cue of the n<sup>th</sup> trial (Extended Data Fig. 3c, bottom panels). The DI shown in  
960 plots has been smoothed with a 200 ms moving average kernel for clarity.

961

962 As expected, normalizing fluorescence to the baseline period (*normalized baseline*) erased the  
963 correlation of baseline dF/F signals with first-lick time (Extended Data Fig. 3c, middle panels).

964 More insidiously, this also resulted in distortion of GCaMP6f dynamics *during* the timing interval,  
965 evident in the diminished difference between E-signals compared to R-signals relative to the  
966 shapes observed in the raw fluorescence paired-trial comparison (Extended Data Fig. 3c, middle-  
967 bottom panel). However, dF/F Methods 2-4 visually and quantitatively recapitulated the dynamics  
968 observed in the raw fluorescence comparison (Extended Data Fig. 3c, right panels).

969  
970 These results were corroborated by time-in-session permutation tests in which datasets for single  
971 sessions were divided into thirds (beginning of session, middle of session, and end of session). The  
972 differences between baseline and ramping dynamics observed in whole-session averages were  
973 present even within these shorter blocks of time within the session (i.e., faster ramping and elevated  
974 baseline signals on trials with earlier self-timed licks). Furthermore, permutation tests in which the  
975 block identity (begin, middle, end) was shuffled showed that this pattern held when trials with  
976 earlier first-licks from the end of the session were compared with trials with later first-licks from  
977 the beginning of the session (and vice versa).

978

979

## 980 **B. Derivation of threshold and alternative decoding models**

### 981 *Derivation of threshold models*

982 As a metric of the predictive power of ramping DAN signals on first-lick time, we derived a  
983 threshold-crossing model. A threshold-crossing event was defined as the first time after the cue  
984 when the photometry signal exceeded and remained above a threshold level up until the time of  
985 first-lick on each trial. Importantly, while the analysis approach is reminiscent of pacemaker-  
986 accumulator models for timing, we make no claims that the analysis is evidence for pacemaker-

987 accumulator models. Rather threshold-crossing times provided a convenient metric to compare the  
988 rate of increase in signals between trials.

989  
990 Photometry timeseries for GCaMP6f and tdt were de-noised by smoothing with a 100ms Gaussian  
991 kernel (kernel was optimized by grid search of kernels ranging from 0, 30, 50, 80, 100, 150, 200  
992 ms to minimize noise without signal distortion). To completely exclude the sensory- and motor-  
993 related transients locked to the cue and the first-lick events, the ramping interval was  
994 conservatively defined as 0.7 s post-cue up until 0.6 s before the first-lick. To eliminate chance  
995 crossings due to noise, we imposed a stiff, debounced threshold condition: to be considered a  
996 threshold crossing event, the photometry signal had to cross the threshold from low-to-high and  
997 remain above this level until the end of the ramping interval.

998  
999 To derive an unbiased threshold for each session, we tested 100 evenly-spaced candidate threshold  
1000 levels spanning the minimum-to-maximum photometry signal during the ramping interval for each  
1001 session. Depending on threshold level, some trials never crossed, i.e., signal always remained  
1002 below threshold or started and ended above threshold. Thus, the lowest candidate threshold for  
1003 which there was a maximum number of trials crossing during the timing interval was selected as  
1004 the “mid-level” threshold-crossing point. This threshold was specific to each photometry signal  
1005 tested on each session. Threshold-crossing time was included in the decoding model as the  
1006 normalized time on the ramping interval (0,1). If a trial never crossed threshold, it was encoded as  
1007 a zero. If no trials ever crossed threshold, the threshold predictor was encoded as a vector of ones,  
1008 thus penalizing the model for an additional predictor but providing no new information.

1009

1010 ***Multi-threshold Model***

1011 An alternative model employed 3 unbiased thresholds: 1) the lowest threshold with  $\geq 50$  trials  
1012 crossing (“min”); 2) the lowest threshold with the most crossings (“mid,” described above); and 3)  
1013 the highest threshold with  $\geq 50$  trials crossing (“max”). For tdt datasets, trials rarely met the  
1014 monotonic threshold constraint (usually the signals oscillated above and below the threshold  
1015 throughout the ramping interval, failing to meet the debouncing constraint). Thus, to include tdt  
1016 signals as conservatively as possible, we relaxed the 50-trial minimum constraint, taking the  
1017 threshold with the most trials crossing, which was usually around 10 or fewer. The addition of  
1018 more thresholds did not substantially improve the cross-validated model compared to the single-  
1019 threshold model (Extended Data Fig. 8c).

1020

1021 ***Principle component analysis (PCA) threshold-crossing models***

1022 In another version of the decoding model, the threshold-crossing procedures were applied to  
1023 ramping intervals fit with the first three PCs (as described in Methods) to derive a PCA version of  
1024 the single-threshold and multi-threshold models. PCA analysis on tdt datasets showed no  
1025 consistent PCs, and thus these PCs were not included in the decoding model. Instead, the actual  
1026 tdt data was employed in the threshold model as in the other models described.

1027

1028

1029

1030

1031

1032

1033 **2. Supplementary Discussion**

1034

1035 **A unifying Reward-Prediction-Error based framework underlying dynamic DAN activity in**  
1036 **timing tasks.**

1037 A framework that has explained many disparate experimental results from the dopaminergic  
1038 system is temporal difference (TD) learning with reward-prediction errors (RPE)<sup>27,33</sup>. In this  
1039 framework, DAN activity is thought to reflect the moment-to-moment difference in the animal's  
1040 expectation versus its perception of the value of its current state, where value is defined as the  
1041 temporally-discounted expectation of total future reward. In classical trace-conditioning  
1042 paradigms, DANs fire in transient bursts to unexpected rewards and reward-predicting cues,  
1043 whereas they pause their firing when expected reward is omitted. Indeed, we observed RPE-like  
1044 signals in the cue-related transient, dips in activity after unrewarded first-licks, and surges in  
1045 activity following rewarded first-licks (Fig. 1c-e, Extended Data Fig. 4a-d). Persistence of RPE-  
1046 like signals in well-trained animals has been suggested to arise from the inherent imprecision in  
1047 neural timing<sup>2</sup>, which may reflect the animal's moment-to-moment uncertainty of its current  
1048 state—i.e., its position in time—and, by extension to our task, uncertainty about its accuracy for a  
1049 given self-timed lick<sup>30</sup>. Indeed, positive-going RPE-like signals were strongest for first-licks  
1050 closest to the reward-boundary, presumably when the mouse's "confidence" of reward was lowest,  
1051 consistent with the greatest RPE occurring when the mice were least certain of success (Extended  
1052 Data Fig. 4a-d).

1053

1054 Whereas RPE-frameworks have explained *transient* bursts and pauses in DAN activity during  
1055 trace conditioning and other types of learning experiments, DAN activity can also change more

1056 slowly<sup>30</sup>. For example, “ramping” signals build up over seconds during goal-directed navigation<sup>19</sup>,  
1057 bandit tasks in which animals must complete multiple goals to receive reward<sup>25,26</sup>, and tasks with  
1058 visual cues of proximity to reward<sup>20</sup>. It has been suggested that DANs could signal different  
1059 information via slow changes in activity (e.g., motivation, ongoing value, vigor) compared to fast-  
1060 timescale activity (e.g., post-hoc RPE signals for learning), and a number of proposals have  
1061 suggested that DANs multiplex different kinds of information over different timescales and  
1062 contexts<sup>21,26</sup>.

1063  
1064 However, recent models have proposed RPE-based explanations that may be able to reconcile  
1065 these seemingly disparate dopamine signals<sup>20,27,30</sup>. While these models do not refute the possibility  
1066 that DANs could encode other types of information (e.g., value, vigor, etc.), they are attractive for  
1067 their parsimonious explanation of how fast time-scale phenomena and slowly-evolving ramps  
1068 could arise from the same underlying RPE-based calculation. In short, these models employ  
1069 principles from TD learning to show how certain shapes of the value function (i.e., the assignment  
1070 of values to the series of behavioral states comprising a task) can give rise to a *continuously*  
1071 *changing* RPE, even in well-trained animals<sup>20,27,30,34</sup>.

1072  
1073 We were interested in whether an RPE-based framework could explain the results found in our  
1074 self-timed movement task as well as results from other timing tasks<sup>1</sup>. To approach this question,  
1075 we applied a key feature of TD learning algorithms to determine what an RPE-like signal would  
1076 look like in different kinds of timing tasks. Specifically, we took advantage of the fact that *RPE is*  
1077 *proportional to the derivative of the subjective value function under conditions of state*

1078 *uncertainty*<sup>27,30</sup>, as is the case during timing tasks in which the animal must rely on its own internal  
1079 representation of time to guide behavior<sup>27</sup>.

1080

1081 Thus, if the value landscape for a given behavioral task is known, and if DAN activity encodes  
1082 RPE, the RPE-based framework makes predictions about the expected shape of dynamic DAN  
1083 activity during the task. In a recent study, similar applications of this principle predicted the  
1084 ramping DAN signals that were observed in virtual reality (VR) tasks in which animals were  
1085 moved passively through VR spaces, as well as when the animals passively viewed abstract,  
1086 dynamic visual cues indicating proximity to reward<sup>20</sup>, suggesting the ramping in our task could be  
1087 explained from similar principles.

1088

1089 *RPE-predictions for DAN responses during self-timed movement.*

1090 In a simple TD learning model of self-timed movement, time may be modeled as a continuous set  
1091 of states through which a Markov agent must traverse to receive reward<sup>35</sup> (Supplementary Fig. 1a).  
1092 At each state transition (timestep), the agent must decide whether to move (lick) or to wait based  
1093 on the probability of transitioning to a reward or failure state. If the agent is an optimal timer, its  
1094 subjective approximation of its current state,  $\tau$ , accurately tracks veridical time,  $t$ , and it will thus  
1095 withhold movement until the first moment at which reward will be available in response to licking  
1096 (3.3 s in our experiment).

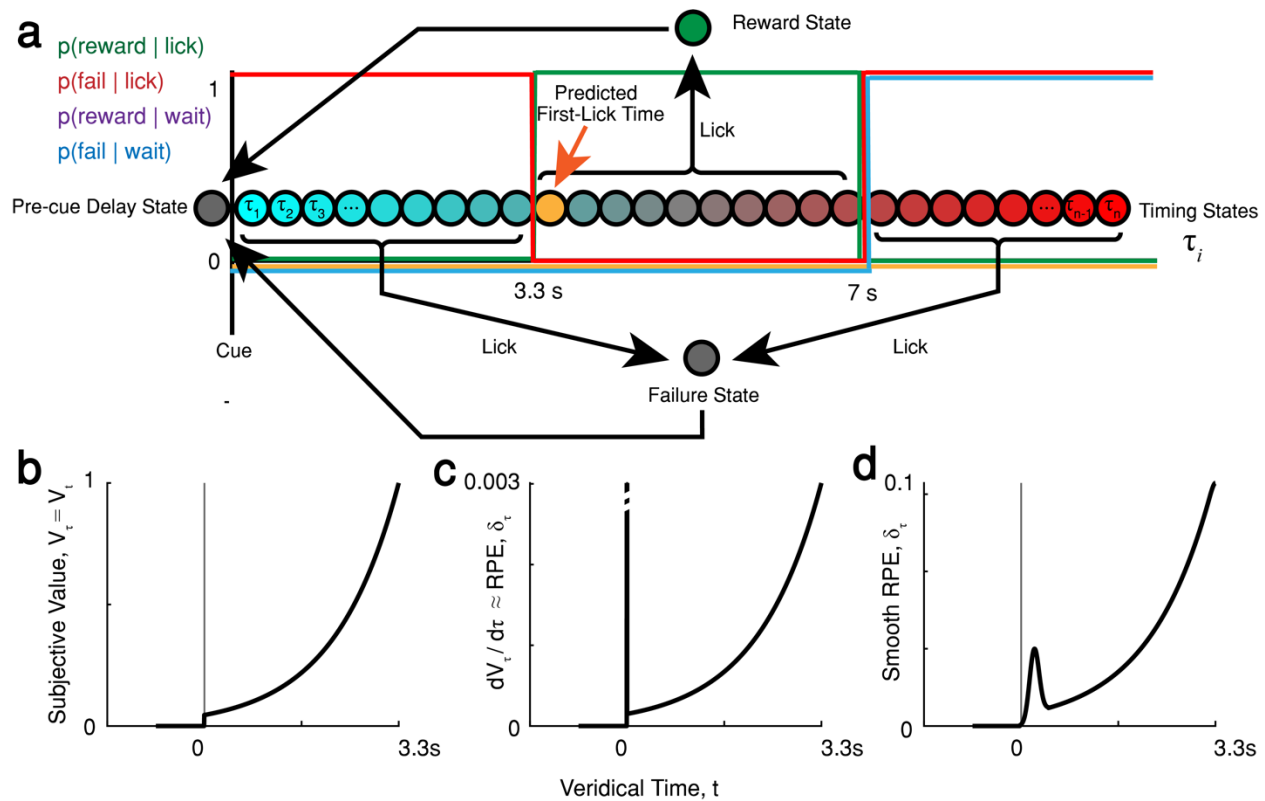
1097

1098 The value landscape of this model can be understood intuitively. When the cue event occurs, a  
1099 well-trained agent can expect an increased possibility of reward in the next few seconds; thus, at  
1100 this moment, value increases. However, reward never occurs within the first 3.3 s of the standard

1101 timing task we implemented; thus, value at the cue is necessarily lower than value at 3.3 s. In fact,  
1102 value will constantly increase as time approaches 3.3 s. Thus, as long as the agent withholds licks,  
1103 the value landscape,  $V_t$ , during the first few seconds is a monotonically increasing, convex  
1104 function<sup>36</sup> (Supplementary Fig. 1b). If the agent is an optimal timer, the subjective approximation  
1105 of the value function,  $\hat{V}_\tau$ , matches the true value function, and  $\hat{V}_\tau = V_t$ .

1106  
1107 However, we assume that, because the timer does not have access to the true state identity,  $t$ , it is  
1108 never certain of its subjective approximation of its state,  $\tau$ . Under conditions of state uncertainty,  
1109 RPE is approximately the derivative of the subjective value function<sup>20,27</sup>,  $\delta_\tau \approx \hat{V}'_\tau$ , where  $\delta_\tau$  is  
1110 RPE at subjective time  $\tau$ , and  $\hat{V}'_\tau$  is the time-derivative of the subjective value function. Thus, the  
1111 shape of the RPE function,  $\delta_\tau$  is also quite simple: a transient increase at the cue followed by a  
1112 slowly-evolving ramp (Supplementary Fig. 1c). If the RPE function is measured by a calcium  
1113 indicator such as GCaMP6f, the binding kinetics of the indicator would tend to blur the RPE  
1114 function, which we approximated by smoothing (Supplementary Fig. 1d).

1115



1116

1117 **Supplementary Figure 1 | Value and RPE Landscapes for an optimal timer predict**

1118 **DAN responses during the self-timed movement task. a**, State space and probability of

1119 state transition for an optimal timer. Gold-shaded state is the first state from which reward is

1120 available, and thus is when the first-lick is predicted to occur. **b**, Estimated value function  $\hat{V}_t$ ,

1121 where  $\hat{V}_t \approx V_t$  for an optimal timer. An exponential value landscape is shown, consistent

1122 with prior literature<sup>27</sup>. However, any sufficiently convex function could be implemented with

1123 the same result<sup>27,30</sup>. The agent is expected to first-lick at the peak of the trajectory. **c**, RPE

1124 function for an optimal timer, estimated as  $\delta_\tau \approx \hat{V}'_\tau$ , the derivative of the subjective value

1125 function. Y-axis scaled to show ramp. **d**, Predicted DAN GCaMP6f signals for an optimal

1126 timer. The RPE function was smoothed with a gaussian kernel spanning *ca.* 10% of the

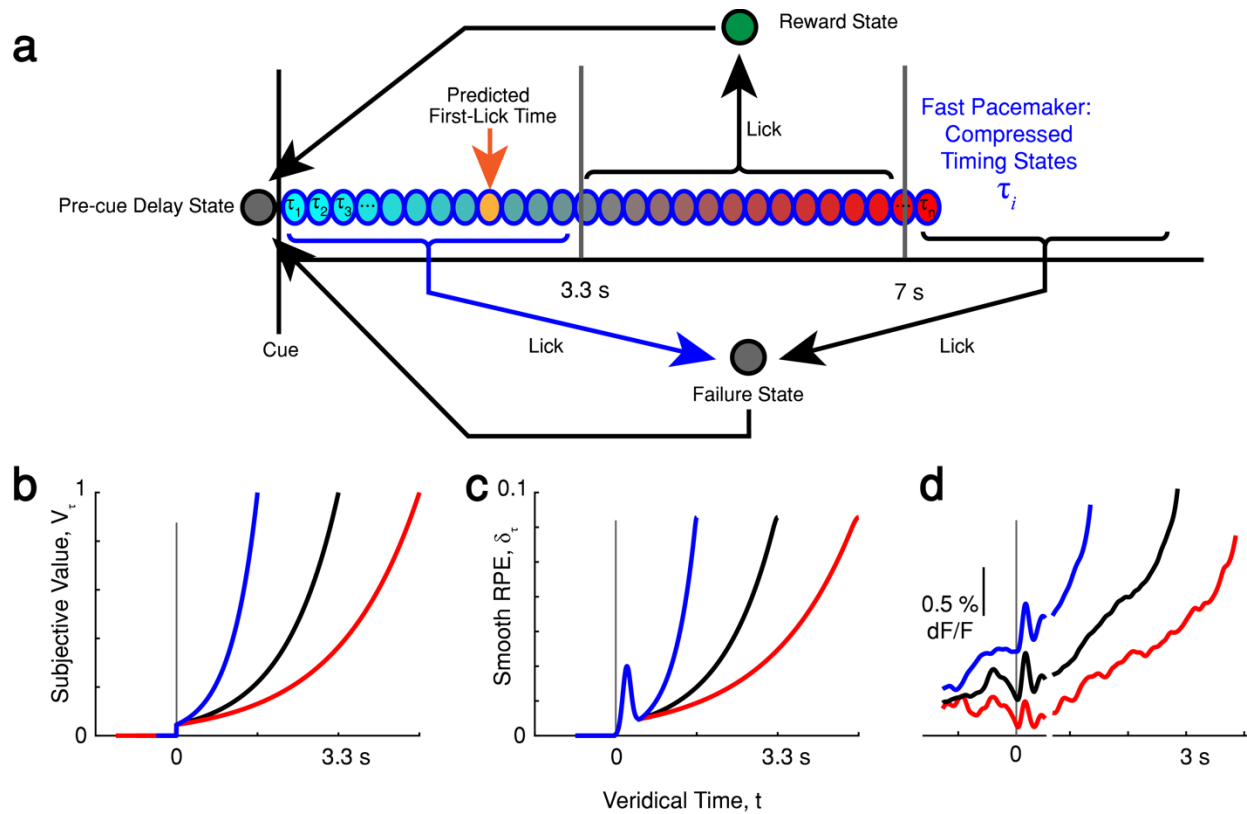
1127 interval to approximate GCaMP6f off-dynamics.

1128

1129 The modeled RPE function mirrors the shape of the dynamics observed in DAN signals: a cue-  
1130 related transient followed by a slow ramp up to the time of first-lick. However, unlike the optimal  
1131 timer in this model, mice, like humans, exhibit suboptimal timing behavior with variability  
1132 proportional to the duration of the timed interval<sup>2</sup>. It has been proposed that this variability in  
1133 timing results from imprecision in an internal clock, referred to classically as the internal  
1134 “pacemaker<sup>37</sup>.” When the pacemaker is fast, self-timed movements occur relatively early, whereas  
1135 when the pacemaker is slow, later movements occur. These changes in the pacemaker rate would  
1136 correspond to the mouse traversing the set of subjective states,  $\tau$ , at different rates than the passage  
1137 of veridical time,  $t$  (Supplementary Fig. 2a), resulting in relative *compression* and *stretching*,  
1138 respectively, in the subjective value function,  $\hat{V}_\tau$  (Supplementary Fig. 2b), with corresponding  
1139 compression/stretching of the RPE function (Supplementary Fig. 2c).

1140

1141



1142

1143 **Supplementary Figure 2 | Compressed and stretched Value and RPE Landscapes for a**

1144 **sub-optimal timer predict dynamic DAN responses during the self-timed movement task,**

1145 **but do not capture baseline offsets. a,** Simple state space of self-timed movement task for a

1146 suboptimal timer with a fast pacemaker. The fast pacemaker “compresses” state space<sup>30,35</sup>,

1147 resulting in traversal of the timing states faster than veridical time. The mouse can only make

1148 a decision based on which state it believes itself in; thus first-lick is expected to occur early

1149 (gold-shaded state). **b,** A compressed subjective value function ( $\hat{V}_{\tau}$ , blue) reflects relatively

1150 fast traversal through the value landscape compared with that of veridical time ( $V_{\tau}$ , black).

1151 Conversely, stretched  $\hat{V}_{\tau}$  (red) reflects slow traversal, consistent with a slow pacemaker. The

1152 animal is expected to lick at the peak of the trajectory. **c,** Smoothed estimated RPE function

1153 ( $\hat{V}'_{\tau} \approx \delta_{\tau}$ ). Compression/stretching of the value function produces ramping dynamics similar

1154 to those observed in DANs (**d**) and striatal dopamine (Fig. 1f). However, this model alone

1155 does not explain the more tonic baseline offsets that were anti-correlated with upcoming  
1156 movement time.

1157

1158 Strikingly, as this simple RPE-based model predicts, DAN signals observed during our self-timed  
1159 movement task show different ramping dynamics depending on when the animal actually moved  
1160 (Supplementary Fig. 2d), consistent with compression/stretching of the subjective value and RPE  
1161 functions. When the animal moved relatively early (perhaps corresponding to a fast pacemaker),  
1162 DAN ramping unfolded with a steeper slope, as if the ramping period were *compressed*.  
1163 Conversely, when the animal moved late (perhaps corresponding to a slow pacemaker), DAN  
1164 ramping unfolded with a shallower slope, as if the ramping interval were *stretched*. The idea of  
1165 compression/stretching of DAN ramps was supported by our encoding model (Fig. 2, Extended  
1166 Data Fig. 7), for which we needed to add a timing-dependent “stretch factor” to best capture the  
1167 variance in GCaMP6f signals during the timed interval. Together, these observations could be  
1168 explained by DANs encoding an RPE-like signal related to the animal’s “belief” of its position in  
1169 objective time,  $\tau$ , as derived from its position along the subjective value trajectory during the  
1170 timing interval of the task.

1171

1172 In fact, a recent model described how a timing mechanism instantiated by the nigrostriatal system  
1173 could lead to (the well-known) variability in self-timed intervals by stretching or compressing of  
1174 subjective value trajectories<sup>30</sup>. The model posits that dopamine modulates the pacemaker rate  
1175 (consistent with pharmacological and lesion studies), with increased dopamine availability (or  
1176 efficacy) speeding the pacemaker, and decreased dopamine slowing the pacemaker<sup>4,5,8-11</sup>. In turn,  
1177 the pacemaker controls the encoding of subjective time, and thus the steepness of the value

1178 function with respect to objective, veridical time. It follows that variation in dopamine availability  
1179 would compress or stretch the value landscape to varying degrees from trial-to-trial. This model is  
1180 consistent with our findings of variable ramping slope in DANs signals from trial-to-trial. It is also  
1181 consistent with neural recordings from striatal spiny projection neurons and parietal cortical  
1182 neurons during similar self-timed movement tasks, for which temporal sequences of striatal and  
1183 cortical firing during timing were compressed for early movements and stretched for late  
1184 movements<sup>6,24</sup>.

1185  
1186 While the RPE-based view of DAN activity captures the dynamic DAN signals we observed, our  
1187 simple RPE model alone does not capture the *baseline offsets* in DAN signals that were predictive  
1188 of movement timing even after controlling for previous trial outcome and ongoing nuisance  
1189 movements (Fig. 3, Extended Data Fig. 6c). More complex RPE-based explanations for these *tonic*  
1190 offsets in DAN signals could be imagined with further assumptions (e.g., states like the pre-cue  
1191 delay could also contain timing states that create offsets before the trial begins, etc.), but a  
1192 parsimonious explanation for how and why these offsets emerge requires further investigation.  
1193 Mohebi *et al.* recently showed baseline differences in the amount of dopamine in the nucleus  
1194 accumbens core that were correlated with the recent history of reward rate: higher recent reward  
1195 rates were related to higher tonic dopamine. However, in our task, animals tended to move later  
1196 toward the end of sessions, resulting in periods of relatively high reward rate when the average  
1197 tonic baseline signal was *lower* (baseline preceding rewarded trials—by definition, later  
1198 movements—was systematically lower in our task, Fig. 1d-f), suggesting a more complex  
1199 relationship between tonic DAN activity and reward rate in our task. While the origin of offsets in  
1200 DAN signals remains unclear, these offsets were nonetheless inversely related to the first-lick time,

1201 and thus directly related to the (inferred) pacemaker rate, consistent with pharmacological and  
1202 lesion studies positing a positive correlation between dopamine availability and pacemaker rate<sup>4-  
1203 5,8-11,30</sup>.

1204  
1205 Ramping signals in our photometry experiments were measured from a population of DANs. An  
1206 important future question is whether ramps are also present at the level of individual neurons, or  
1207 rather represent a progressive recruitment of individual neurons, or some combination of both.  
1208 Prior studies have reported ramping signals in individual neurons during tasks with visual feedback  
1209 of distance to reward<sup>20</sup>, whereas others have observed decoupling between DAN firing rates and  
1210 downstream DA release<sup>26</sup>, making it unclear whether electrophysiology would be capable of  
1211 addressing this question. Observation of individual neurons expressing calcium indicators with  
1212 GRIN-lens equipped endoscopes may be better suited to this question.

1213

1214 *RPE-based predictions for DAN responses during a temporal bisection task.*

1215 Whereas DAN signals during our self-timed movement task were consistent with classic  
1216 observations of the influence of dopamine on the speed of the pacemaker, a recent study employing  
1217 a different timing task found more complex DAN dynamics during timing. Soares *et al.* recorded  
1218 SNc DAN GCaMP6f signals with fiber photometry as mice executed a classic temporal bisection  
1219 perceptual task<sup>1</sup> (Supplementary Fig. 3a). Trials began when mice entered a nose-poke port and  
1220 received an auditory start-timing cue. Mice had to remain in the port throughout a variable timing  
1221 interval, which was terminated with a stop-timing auditory cue. Mice then reported whether the  
1222 interval was shorter or longer than a criterion time (1.5 s) by choosing a left or right nose-poke  
1223 port corresponding to a “long” or “short” judgment. Mice were trained to categorize intervals

1224 spanning 0.6-2.4 s. As expected, trials with more extreme intervals were easier for the mice,  
1225 whereas trials with intervals closer to the 1.5 s criterion time elicited chance performance  
1226 (Supplementary Fig. 3b).

1227

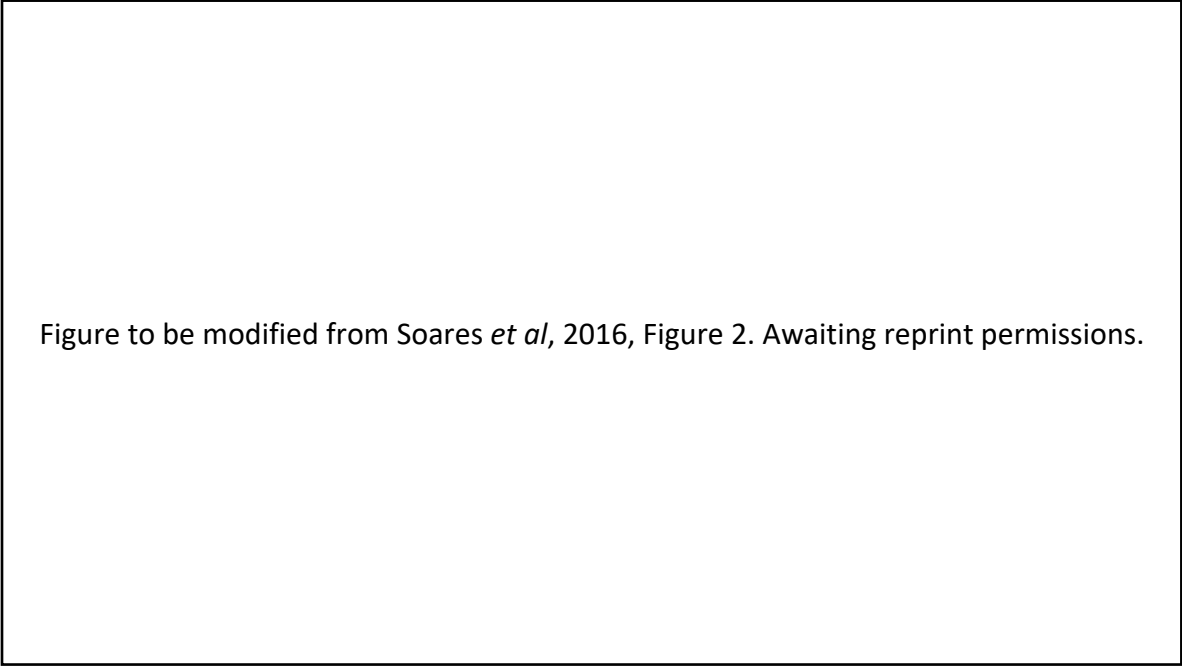


Figure to be modified from Soares *et al*, 2016, Figure 2. Awaiting reprint permissions.

1228

1229 **Supplementary Figure 3 | A temporal bisection task shows relatively high DAN signals**  
1230 **during the timing interval when the inferred pacemaker rate is relatively fast.** Figures  
1231 adapted from Soares *et al.*, 2016<sup>1</sup>. **a**, Task schematic. **b**, Psychometric curve for timing  
1232 intervals of different duration. Criterion time: 1.5 s. **c**, Start-timing cue-aligned average SNc  
1233 DAN GCaMP6f signals. Second peak occurs just after the stop-timing cue (intervals: 0.6,  
1234 1.05, 1.26, 1.74, 1.95, 2.4 s). Figure recolored to indicate average inferred pacemaker rate.  
1235 Red: slow; blue: fast. Relative dF/F amplitude during baseline and immediately prior to stop-  
1236 timing cue shown left and right. dF/F amplitudes during timing are higher when the inferred  
1237 pacemaker rate is fast. Left: Correct trials. Right: Incorrect trials show the same dF/F  
1238 relationship with pacemaker rate.

1239  
1240 DANs exhibited complex dynamics during the bisection task, starting with a sharp transient after  
1241 the start-timing cue and ending with second transient after the stop-timing cue (Supplementary Fig.  
1242 3c). Between the start-timing and stop-timing cues, DAN signals exhibited a U-shape with  
1243 increasing time, which was visible for trials with longer intervals but was truncated prematurely  
1244 for the shorter intervals. The authors focused their analyses on the transient occurring *after the*  
1245 *stop-timing* cue. Short judgments (suggesting a slow pacemaker) were accompanied by relatively  
1246 high-amplitude transients after the stop-cue, whereas long judgments (suggesting a fast pacemaker)  
1247 showed relatively low-amplitude transients. These results seemed to suggest that relatively *high*  
1248 DAN activity reflected a *slow* pacemaker, the opposite of what is expected based on the bulk of  
1249 pharmacological and lesion studies<sup>30</sup>, as well as the trend we observed during our self-timed  
1250 movement task.

1251  
1252 This surprising finding could be a unique feature of the bisection task. Unlike self-timed  
1253 movements, in which animals directly report elapsed time with a movement, the temporal bisection  
1254 task requires an additional computational step, in which the timed interval must be categorized as  
1255 “long” or “short.” However, prior pharmacological studies employing the bisection task found  
1256 results consistent with the classic view that higher dopamine availability is associated with a faster  
1257 pacemaker<sup>30,38</sup>—opposite the interpretation of Soares *et al.*, but consistent with the findings of our  
1258 self-timed movement task.

1259  
1260 The discrepancy between our results and those found by Soares *et al.* could perhaps be traced to  
1261 differences in the way DAN signals were analyzed. We focused our attention on DAN signals

1262 unfolding *during timing* in our self-timed movement task, whereas these signals were not explored  
1263 by Soares *et al.* We thus asked two questions: 1. What correlations exist between DAN signals and  
1264 pacemaker rate in the bisection task *before* the timing interval? And, 2. What correlations exist  
1265 *during* the timing interval itself?

1266  
1267 Before addressing these questions, we note that the relationship between pacemaker and bisection  
1268 judgment is not as straightforward as in self-timed movement, and thus we recolored  
1269 Supplementary Fig. 3c to clarify this, employing the following intuition: For a trial to be correct  
1270 in the bisection task, on average, the pacemaker must be either accurate or “conservatively  
1271 inaccurate.” In other words, a correct “short” judgment requires either accurate timing or a *slow*  
1272 pacemaker (Supplementary Fig. 3c, red curves). Conversely, a correct “long” judgment requires  
1273 either accurate timing or a *fast* pacemaker (Supplementary Fig. 3c, blue curves).

1274  
1275 When we considered DAN signals *before* the timing interval for correct trials in the Soares *et al.*  
1276 study (Supplementary Fig. 3c, left), we noticed what appears to be two strata of signal levels. Trials  
1277 with “long” judgments (fast pacemaker on average) had relatively high baseline signals, whereas  
1278 trials with “short” judgments (slow pacemaker on average) had lower baseline signals, consistent  
1279 with the relationship between baseline offsets and pacemaker rate that we observed in our self-  
1280 timed movement task. As in our task, these baseline offsets remained present during the timing  
1281 interval, resulting in the same stratification of dF/F signals immediately prior to the stop-timing  
1282 cue (except for the very earliest time, 0.6s, which overlaps decaying GCaMP6f signals related to  
1283 the start-timing cue, likely causing an artifactual inflation of the signal just prior to the stop-cue  
1284 due to the off-kinetics of the calcium indicator or kinetics of calcium clearance more generally).

1285 Thus, it generally appears that DAN activity was *higher* on trials with fast pacemaker rates, both  
1286 during and before the interval in which the animal was actually timing. Intriguingly, *incorrect*  
1287 trials (to the right in Supplementary Fig. 3c) showed a relative convergence of the baseline signals  
1288 preceding the start-cue, but then signals diverged during the timing interval, resulting in relatively  
1289 *high* signals at the time of the stop-cue for incorrect “long” choices (i.e., a fast pacemaker), but  
1290 relatively low signals at the time of the stop-cue for incorrect “short” choices (i.e., a slow  
1291 pacemaker). This is consistent with the patterns observed on correct trials. Interpreted thusly, the  
1292 Soares *et al.* result is consistent both with our results and with classic pharmacological studies  
1293 relating higher/lower dopamine availability to faster/slower pacemaker rates, respectively. Soares  
1294 *et al.* presented their subsequent analyses with these baseline differences normalized-out in some  
1295 way (Fig. 3 of Soares *et al.*). It is possible that this “zeroing out” of the baseline offset may have  
1296 hindered efforts to detect consistent effects during the timing interval due to reordering of the  
1297 traces.

1298  
1299 Because baseline offsets in the bisection task appear similar to those in our self-timed movement  
1300 task, we asked whether dynamic DAN signals in the bisection task could similarly be explained  
1301 by the task’s RPE landscape. In their investigation of the stop-timing cue-related transient, Soares  
1302 *et al.* showed that its amplitude is well-explained by a combination of temporal surprise and  
1303 behavioral performance, and we applied these parameters to derive a value landscape consistent  
1304 with their bisection task.

1305  
1306 The inferred value landscape of the bisection task for an optimal agent was built from a few  
1307 assumptions (Supplementary Fig. 4a):

1308

1309 1. As in our self-timed movement task, value increases immediately at the start-cue and  
1310 continues to rise toward the time of expected potential reward delivery.

1311

1312 2. Because the longest interval is 2.4 s, the time until potential reward is known to be no more  
1313 than ~3 s (including the time to report judgment). However, due to temporal uncertainty  
1314 and the fact that a false start (leaving the port before the stop-timing cue) results in an error  
1315 and loss of reward, there is a second jump in the value function at the time of the stop-cue  
1316 when the feedback of the tone reorients the value function and indicates the opportunity to  
1317 collect reward within a few hundred milliseconds.

1318

1319 3. Because value is temporally discounted at the start-cue by the possibility of the longest-  
1320 possible interval, any stop-cue occurring before 2.4 s results in a sudden “teleportation”  
1321 through the value landscape to the final limb of the task that occurs just before the judgment  
1322 and ascertainment of trial outcome, similar to the jump in the value function in a recently-  
1323 reported, virtual reality, spatial teleportation task<sup>20</sup>. Thus, assuming the value function  
1324 trends upwards steadily, the amplitude of RPE-related transients following the stop-cue  
1325 would *decrease* as the interval duration increases, because the sudden jump in the value  
1326 function becomes progressively smaller.

1327

1328 4. To capture aspects related to behavioral performance, we additionally included contours in  
1329 the value function during the timing interval to reflect the probability of a correct choice  
1330 for intervals of different lengths. Specifically, a relative minimum in the value function

1331 occurs near 1.5 s, when predicted performance is worst. However, a stop-timing tone near  
1332 the criterion time also results in a smaller jump in the value function because the probability  
1333 of a correct decision is also lower. Thus, the increase in value at the moment of decision  
1334 was adjusted by the probability of a correct choice.

1335

1336 5. As in the simple RPE-model of our self-timed movement task, we modeled changes in  
1337 pacemaker rate as compression/stretching of the subjective value landscape with respect to  
1338 veridical time.

1339

1340 6. The agent traverses timing states during the timing interval, similar to the timing states in  
1341 the self-timed movement task, but unlike our task, the bisection task does not require the  
1342 agent to decide when to move. We assume the need to make a timed movement imposes a  
1343 need for the agent to be relatively certain of its subjective timing state,  $\tau$ , to make a decision,  
1344 even though it is uncertain of its true state,  $t$ . The bisection task, on the other hand, is more  
1345 similar to classical conditioning tasks in which the timing interval is not in the agent's  
1346 control, and thus subjective state uncertainty increases with the distance from the last state-  
1347 informative cue<sup>30</sup>. Thus, we took into account temporal blurring of the subjective state  
1348 function, which would tend to reduce the convexity of the subjective value function and  
1349 reduce the amplitude of ramping during the timing interval<sup>30</sup>. However, adding temporal  
1350 blurring does not substantially change the fit-shape in our simplified model, and versions  
1351 with or without blurring can reproduce the shape of the dynamic DAN signals.

1352

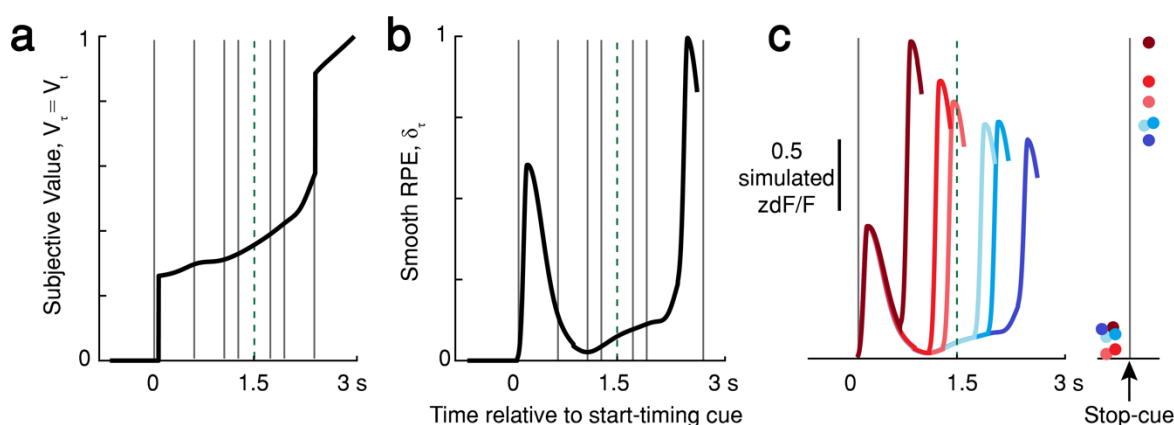
1353 Together, we arrived at a model of the RPE landscape for each of the six tested interval durations  
1354 (Supplementary Fig. 4b,c). Importantly, this simple RPE-based model accurately captures the  
1355 relative categorical amplitudes of the stop-timing cue-related transients, as follows: If the  
1356 instantaneous DAN activity at the time of the stop-timing cue is relatively high, this would indicate  
1357 that the animal is further along in the subjective value trajectory, resulting in 1) a *long* judgment,  
1358 and 2) a relatively *smaller* RPE transient, because the underlying subjective value was higher at  
1359 that moment. Conversely, if instantaneous DAN activity is relatively low at the stop-timing cue,  
1360 this this would indicate that the animal is not very far along the subjective value trajectory, leading  
1361 to 1) a *short* judgement and 2) a relatively *larger* stop-cue-related RPE transient, because the  
1362 underlying subjective value was relatively low just before the stop-cue.

1363  
1364 Now consider a particular (objective) time interval near the criterion time, for which the animal  
1365 makes a mix of “long” and “short” choices (e.g., 1.74s; Supplementary Fig, 3b). Soares *et al.* found  
1366 that the amplitude of the stop-timing cue-related GCaMP6f transient tended to be bigger when the  
1367 animal made short choices, and this was taken as evidence that elevated DAN activity *slows* the  
1368 internal clock. However, our model predicts that the size of the stop-cue-related transient will be  
1369 inversely related to the amplitude of the underlying subjective value at that point, and thus  
1370 inversely related to elapsed *subjective* time. It thus follows that if subjective time is more advanced  
1371 on a given trial (i.e., faster pacemaker), the animal would tend to choose the long judgment on that  
1372 trial, and the stop-timing RPE transient would be *smaller*. Conversely, if subjective time is less  
1373 advanced on a trial (i.e., slower pacemaker), the animal would tend to choose the short judgment,  
1374 and the stop-timing RPE transient would be *larger*.

1375

1376 Our RPE model accurately predicts the results of Soares *et al.*; however, our model holds that  
1377 elevated DAN activity *speeds* the internal clock, consistent with most pharmacological studies but  
1378 *opposite* the interpretation of Soares *et al.* Thus, our RPE-based model suggests a parsimonious  
1379 explanation for DAN activity in both the self-timed movement and temporal bisection paradigms,  
1380 with (1) relatively high DAN activity corresponding to a fast pacemaker; manifesting in (2)  
1381 compression of the value landscape; thereby leading to (3) early movements (in the self-timed  
1382 movement task) or long judgments (in the temporal bisection task).

1383



1384

1385 **Supplementary Figure 4 | Subjective Value and RPE Landscapes for the temporal**  
1386 **bisection task predict dynamic DAN responses during the temporal bisection task, but**

1387 **do not capture baseline offsets. a**, Estimated value function  $\hat{V}_t$ , where  $\hat{V}_t \approx V_t$  for an  
1388 optimal timer on a 2.4 s trial. Grey lines: test interval times. Green dashed line: criterion time  
1389 (1.5 s). Value increases approaching the time when reward is available, increasing abruptly  
1390 at the start- and stop-timing cues (0 and 2.4 s). **b**, Smoothed RPE function for an optimal  
1391 timer, estimated as  $\delta_t \approx \hat{V}'_t$ , the derivative of the subjective value function. The RPE  
1392 function was smoothed with an asymmetrical gaussian kernel spanning *ca.* 28% of the  
1393 interval to approximate GCaMP6f off-dynamics. **c**, Predicted DAN GCaMP6f signals for an

1394 optimal timer for the six test interval times. Traces truncated before reward collection for  
1395 clarity. Right: relative simulated dF/F amplitude prior to the stop-timing cue and subsequent  
1396 peak response. Amplitude before the stop-timing cue is directly proportional to clock speed;  
1397 amplitude at the stop-timing cue-related peak is inversely proportional to clock speed.

1398

### 1399 **Limitations of the RPE-based model.**

1400 The simple RPE-based models presented here explain dynamic DAN signals in both the bisection  
1401 task and our self-timed movement task, but they do not explain the origin of baseline offsets.  
1402 Mohebi *et al.*<sup>26</sup> recently-proposed that baseline offsets in ventral striatal dopamine levels could  
1403 reflect the average recent reward rate, but we found that offset amplitude in DAN signals is at least  
1404 partially independent of recent trial history during the self-timed movement task. It is possible that  
1405 baseline variation arises from slow, random fluctuations in DAN activity, but further work is  
1406 needed to explore the origins of these signals.

1407

1408 A second issue is the impact of optogenetic DAN activation and suppression on the rate of the  
1409 pacemaker. In our self-timed movement task, DAN activation promoted early movements,  
1410 consistent with increasing the pacemaker rate, whereas suppression promoted late movements,  
1411 consistent with slowing the pacemaker rate (Fig. 4). However, Soares *et al.* reported an opposite  
1412 effect for optogenetic manipulation during the bisection task, at least for DAN activation.

1413

1414 This difference between the tasks could be reconciled by a recent theoretical model proposed by  
1415 Mikhael and Gershman to explain the behavior of the pacemaker in a wide range of classical  
1416 conditioning and timing studies<sup>30</sup>. Their model shows that the pacemaker rate is expected to be

1417 updated at the time of reinforcement by a Hebbian-like, bidirectional learning rule. If reward  
1418 occurs exactly at the expected time, there is no update in the pacemaker rate. However, if  
1419 reinforcement occurs before the expected time, this is interpreted as feedback that the pacemaker  
1420 was running too slowly; thus, the update rule increases the pacemaker rate leading to expectation  
1421 of reward at an earlier time on the next trial. Conversely, if reinforcement occurs after it was  
1422 expected, this is interpreted as feedback indicating an overly fast pacemaker, resulting in an update  
1423 that slows the pacemaker and expectation of a later reward on the next trial. The same principles  
1424 apply to ongoing RPE during timing tasks.

1425 In our self-timed movement task, we activated or inhibited DANs only *up to* the time of first-lick,  
1426 which Mikhael and Gershman's model predicts will produce an effect on the pacemaker rate  
1427 consistent with the sign of the manipulation (activate: increase, inhibit: decrease). However, Soares  
1428 *et al.* continued optical stimulation *past* the end of the timing interval, until the end of the trial.  
1429 When Mikhael and Gershman modeled stimulation in the Soares *et al.* task, they found that  
1430 simulated DAN activation increased the pacemaker rate during the timing interval, but the  
1431 continuing stimulation after the stop-timing cue rapidly counteracted this effect, resulting in  
1432 *slowing* of the modeled pacemaker between the stop-cue and the judgment, leading an effect on  
1433 pacemaker rate *inconsistent* with the sign of the manipulation, as observed in Soares *et al.* If this  
1434 model is correct, the effect of stimulation on the animal's judgment in the Soares *et al.* task may  
1435 have arisen due to continued manipulation of DAN activity *after* the timing interval had ended. A  
1436 "retrospective" effect of this sort might seem counterintuitive, but such retrospective effects have  
1437 long been observed in perceptual studies, in which recall of sensory stimuli can be enhanced by  
1438 additional sensory cues presented shortly after stimulus offset, suggesting that sensory events are  
1439 "buffered" briefly and can be altered by neural activity occurring between the sensory event and

1440 the perceptual decision<sup>39,40</sup>. It is possible that a similar process could occur in the bisection task if  
1441 DAN stimulation extends past the timing interval, although this is speculative. More work is  
1442 needed to reconcile the optogenetic results in the self-timed movement and bisection tasks. To  
1443 start, it would be informative to repeat the optogenetic experiments in the bisection task with  
1444 optical stimulation limited to the period of the timed intervals only.

### 1445 3. Supplementary References

- 1446 33. Schultz, W., Dayan, P. & Montague, P. R. A neural substrate of prediction and  
1447 reward. *Science* **275**, 1593–1599 (1997).
- 1448 34. Starkweather, C. K., Babayan, B. M., Uchida, N., & Gershman, S. J. Dopamine  
1449 reward prediction errors reflect hidden-state inference across time. *Nat. Neuro.* **20**,  
1450 581–589 (2017).
- 1451 35. Sutton, R. S., & Barto, A. G. *Reinforcement Learning*. (2000).
- 1452 36. Gershman, S. J. Dopamine Ramps Are a Consequence of Reward Prediction  
1453 Errors. *Neural Comp.* **26**, 467–471 (2014).
- 1454 37. Gibbon, J., Malapani, C., Dale, C. L., & Gallistel, C. Toward a neurobiology of  
1455 temporal cognition: advances and challenges. *Curr. Opin. Neurobiol.* **7**, 170–184  
1456 (1997).
- 1457 38. Morgan, L., Killeen, P.R., Fetterman, J.G. Changing rates of reinforcement perturbs  
1458 the flow of time. *Behav. Processes* **30**, 259–271 (1993).
- 1459 39. Gegenfurtner, K. R., & Sperling, G. Information Transfer in Iconic Memory  
1460 Experiments. *J. Exp. Psych: Human Perception and Performance* **19**, 845–866 (1993).

- 1461 40. Herrington, T. M., & Assad, J. A. Neural activity in the middle temporal area and lateral  
1462 intraparietal area during endogenously cued shifts of attention. *J. Neurosci.* **29**, 14160–  
1463 14176 (2009).